Acta Mech 231, 1977–2010 (2020)
https://doi.org/10.1007/s00707-020-02623-9

ORIGINAL PAPER

Rabab A. Shanab · Salwa A. Mohamed ·
Norhan A. Mohamed · Mohamed A. Attia

Comprehensive investigation of vibration of sigmoid and power law FG nanobeams based on surface elasticity and modified couple stress theories

Received: 21 December 2018 / Revised: 17 November 2019 / Published online: 22 February 2020

Abstract Based on the modified couple stress theory and Gurtin–Murdoch surface elasticity theory, a size-dependent Timoshenko beam model is developed for investigating the nonlinear vibration response of functionally graded (FG) micro-/nanobeams. The model is capable of capturing the simultaneous effects of microstructure couple stress, surface energy, and von Kármán's geometric nonlinearity. Sigmoid function and power law homogenization schemes are used to model the material gradation of the beam. Hamilton's principle is exploited to establish the nonclassical nonlinear governing equations and corresponding higher-order boundary conditions. To account for the nonhomogeneity in boundary conditions, the solution of the problem is split into two parts: the nonlinear static response with the nonhomogeneous boundary conditions and the nonlinear dynamic response. The resulting boundary conditions for the dynamic response are homogeneous, and so Galerkin's approach is applied to reduce the set of PDEs to a nonlinear system of ODEs. The generalized differential quadrature method in terms of spatial variables is applied to obtain the static response and linear vibration mode. Considering the nonlinear system of ODEs in terms of time-related variables, both pseudo-arclength continuation and Runge–Kutta methods are used to obtain the nonlinear free vibration behavior of FG Timoshenko micro-/nanobeams with simply supported and clamped ends. Verification of the proposed model and solution procedure is performed by comparing the obtained results with those available in the open literature. The effects of the nonhomogeneous boundary conditions, surface elasticity modulus, surface residual stress, material length scale parameter, gradient index, and thickness on the characteristics of linear and nonlinear free vibrations of sigmoid function and power law FG micro-/nanobeams are discussed in detail.

1 Introduction

Functionally graded materials (FGMs) are an advanced generation of composite materials fabricated by varying the volume fractions of the constituents along a specific spatial direction, usually over the thickness of a structure. The gradation of material composition can create a nonhomogeneous composite with continuous and smooth properties. Thus, the FGMs have some striking advantages over traditional composite structures such as bearing high temperature gradients, reducing thermal and residual stresses, and eliminating the concentration of stress that occurred in conventional laminated composites [1]. Nowadays, with the development of the material technology, FGMs have been employed in micro-/nanoelectromechanical systems (MEMS/NEMS) such as atomic force microscopes, thin films in the form of shape memory alloys and micro-sensors [2–4]. However, the size effect plays a major role in the mechanical behavior of such small-scale structures, and

R. A. Shanab · S. A. Mohamed · N. A. Mohamed
Engineering Mathematics Department, Faculty of Engineering, Zagazig University, Zagazig 44519, Egypt

M. A. Attia (✉)
Mechanical Design and Production Engineering Department, Faculty of Engineering, Zagazig University, Zagazig 44519, Egypt
E-mail: omarmadly@yahoo.com; mohadlyattia@yahoo.com

consequently, an accurate mathematical model of FGM structures is a key issue for successful analysis and design of MEMs/NEMs. The effective mechanical properties of the FGMs can be obtained using different homogenization techniques such as exponential, power law, Mori–Tanaka, symmetric power law, and sigmoid function.

At the micro-/nanoscale, the classical continuum mechanics theories cannot correctly predict the experimentally detected size-dependent behavior of structures. To capture this behavior, more general higher-order continuum mechanics theories have been applied, which include strain gradient or couple stress theories that contain additional material constants beside the classical Lamé constants. In the modified couple stress theory (MCST), the stress tensor is symmetric, and only one material length scale parameter is involved to describe the microstructure-dependent size effect, which makes the MCST easier to use than the other higher-order continuum mechanics theories. Since then, the MCST has been widespread applied to investigate the mechanical behavior of micro-/nanoscale structures by researchers [5–14]. According to these microstructure–dependent models, the couple stress effect leads to an increased stiffness of FG micro-/nanobeams.

In nanoscale structures, there is a significantly increased ratio of surface area to bulk volume, which is considered one of their most important characteristics. In spite of ignoring the surface energy effect in classical mechanics, as it is small compared to the bulk energy, the surface energy should not be neglected due to its significant contribution to the total energy of nanostructures. The presence of surface stress (surface tension) results in nonclassical boundary conditions, which have a significant effect in analyzing the nanostructures. Gurtin and Murdoch [15,16] presented a surface elasticity model in which the surface energy effect on the elastic behavior of materials is incorporated. Following the Gurtin and Murdoch model, many studies have been developed to model and analyze the effect of size-dependent surface energy on linear/nonlinear bending, buckling, and vibration responses of elastic nanobeams [17–36], viscoelastic nanobeams [37,38], and piezoelectric and cylindrical nanoshells [31,39–41].

Few models have been reported in the literature to investigate the simultaneous effects of couple stress and surface energy on the mechanical behavior of homogeneous nanobeams [22,23,42–45] and nanoplates [46–51]. Recently, Attia [20] and Shanab et al. [8] have developed nonclassical continuum models for FG nanobeams considering the combined effects of couple stress and surface energy.

Various approaches exist for solving the governing equations of the nonlinear vibration of nanobeams. Approximate solutions for the nonlinear free and forced vibration of Euler–Bernoulli FG nanobeams were obtained using the multiple scale (MS) method [25,26,52,53], Hamiltonian approach [54], or Jacobi elliptic functions [24,27]. On the other hand, numerical methods such as FEM, GDQM, pseudo-arclength continuation, and reduced order method are very efficient to obtain the linear and nonlinear responses of nanostructures. For example, Kasirajan et al. [28] used FEM to obtain the nonlinear vibration of a nonlocal Timoshenko beam considering surface effects. Nonlinear free vibration of a homogeneous Timoshenko beam was studied using the pseudo-arclength method by Ansari et al. [18].

It is seen that the nonlinear vibration of sigmoid and power law functionally graded nanobeams incorporating the simultaneous effects of microstructure and surface energy has not been comprehensively studied. Thus, this paper aims to develop a dynamic nonlinear nonclassical continuum model to study the linear and nonlinear free vibration behaviors of sigmoid and power law FG nanobeams based on the von Kármán's geometric nonlinearity, modified couple stress theory, and surface elasticity theory. The nonlinear nonclassical governing equations and corresponding boundary conditions are derived using Hamilton's principle in the framework of Timoshenko beam theory. Unlike most previous studies, the present model considers the nonclassical (nonideal) boundary conditions due to the presence of both residual surface stress and the material nonhomogeneity. To solve the resulting equations, the solution is partitioned into static and dynamic responses. The static response accounts for the nonhomogeneous boundary conditions such that the resulting boundary conditions for the dynamic response are homogeneous, and so Galerkin's approach can be applied. Moreover, a generalized differential quadrature method (GDQM) is used to discretize the developed model without neglecting any of its nonlinearities in governing equations and boundary conditions. After applying Galerkin's approach, the resulting nonlinear second-order ODE system is solved by two methodologies, namely pseudo-arclength continuation and Runge–Kutta method. The developed model is validated by comparing the present results with the results from the available literature, and good agreement is found. A comprehensive parametric study is presented and discussed in detail to demonstrate the influences of the bulk modulus of elasticity ratio, surface elasticity modulus, surface residual stress, material length scale parameter ratio, dimensionless material length scale parameter, gradient index, nonclassical boundary conditions, and beam thickness on the linear and nonlinear free vibrations of Timoshenko power law and sigmoid FG micro-/nanobeams.

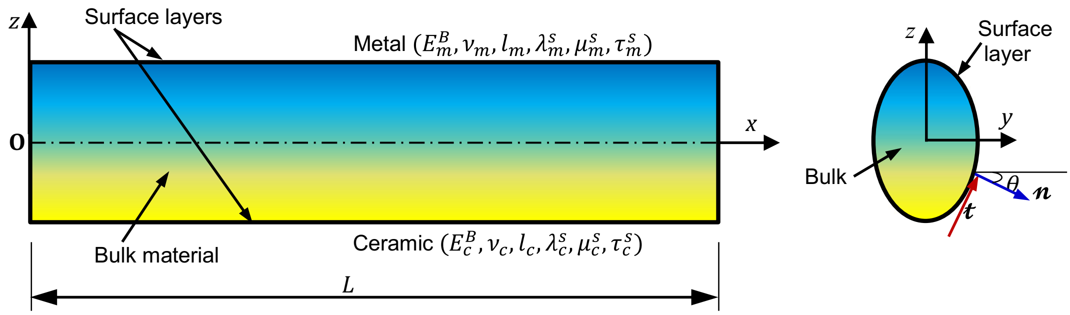

Fig. 1 Schematic of a functionally graded nanobeam with surface layer

2 Theoretical formulation

2.1 Functionally graded materials

One of the main tasks in material mechanics is to correctly predict the material behavior, which requires estimating (homogenizing) the effective mechanical properties of FGMs. There are different homogenization techniques for FGMs such as exponential, power law, Mori–Tanaka, symmetric power law, and sigmoid function. In the present study, both power law (PL-FG) and sigmoid function (SIG-FG) are adopted as homogenization schemes for the FGM beam under consideration. Considering an FGM nanobeam with a rectangular cross section of length L, width b, and thickness h, the nanobeam is assumed to be made of ceramic and metal. The material at the bottom surface ($z = -h/2$) is pure ceramic and at the top surface ($z = h/2$) is pure metal, as depicted in Fig. 1. Through the beam thickness, the proposed distributions of volume fractions of metal and ceramic follow PL-FG and SIG-FG. Then, the effective local material property of bulk material ($\mathcal{P}^B$) such as Young's modulus (E^B), Poisson's ratio (ν^B), mass density (ρ^B), and microstructure material length scale (l) of a PL-FG nanobeam can be described as follows:

$$\mathcal{P}^B(z) = \mathcal{P}_\mathrm{c}^B + \left(\mathcal{P}_\mathrm{m}^B - \mathcal{P}_\mathrm{c}^B\right)\left(\frac{1}{2} + \frac{z}{h}\right)^k, \quad -\frac{h}{2} \le z \le \frac{h}{2}, \tag{1}$$

and for SIG-FG nanobeam, the effective local material property of bulk material can be expressed by (Chi and Chung [55]):

$$\mathcal{P}^B(z) = \begin{cases} \mathcal{P}_\mathrm{c}^B + \frac{1}{2}\left(\mathcal{P}_\mathrm{m}^B - \mathcal{P}_\mathrm{c}^B\right)\left(1+\frac{2z}{h}\right)^k, & -\frac{h}{2} \le z \le 0, \quad (2.1) \\ \mathcal{P}_\mathrm{m}^B - \frac{1}{2}\left(\mathcal{P}_\mathrm{m}^B - \mathcal{P}_\mathrm{c}^B\right)\left(1-\frac{2z}{h}\right)^k, & 0 \le z \le \frac{h}{2}. \quad (2.2) \end{cases}$$

In this study, the effective local material property of surface material ($\mathcal{P}^\mathrm{s}$) such as surface Lamé's constants (λ^s and μ^s), surface residual stress (τ^s), and surface mass density (ρ^s) of the FG nanobeam is described in terms of PL-FG law as follows:

$$\mathcal{P}^\mathrm{s}(z) = \mathcal{P}_\mathrm{c}^\mathrm{s} + \left(\mathcal{P}_\mathrm{m}^\mathrm{s} - \mathcal{P}_\mathrm{c}^\mathrm{s}\right)\left(\frac{1}{2} + \frac{z}{h}\right)^k, \quad -\frac{h}{2} \le z \le \frac{h}{2}. \tag{3}$$

In Eqs. (1–3), $\mathcal{P}_\mathrm{c}$ and $\mathcal{P}_\mathrm{m}$ are the corresponding material properties at the lower (ceramic) and upper (metal) surfaces of the FG beam, respectively. In addition, superscripts "B" and "s" denote the bulk and surface materials, respectively, and k stands for the gradient index which controls the material variation through the beam thickness.

2.2 Kinematics and constitutive relations

According to Timoshenko beam theory (TBT), the displacement field for an arbitrary point can be defined as:

$$u_x(x,z,t) = u(x,t) - z\psi(x,t), \quad u_y(x,z,t) = 0, \quad u_z(x,z,t) = w(x,t) \tag{4}$$

where u and w are the axial and lateral displacements of any point (x, z) on the mid-plane, $\psi\,(x, t)$ is the rotation of the beam cross section with respect to the vertical direction, and t denotes time.

The nonlinear Green–Lagrangian strain tensor (E_{ij}) is defined as follows [56]:

$$E_{ij} = \frac{1}{2}\left[u_{i,j} + u_{j,i} + u_{k,i}u_{k,j}\right] \tag{5}$$

where u_i are the displacement components given by Eq. (4) Throughout the paper, the summation convention and standard index notation are used, with the Greek indices running from 1 to 2 and the Latin indices from 1 to 3 unless otherwise indicated.

On the basis of von Kármán geometric nonlinearity, i.e., only squares of the slopes $u_{z,x}^2$, $u_{z,y}^2$, and $u_{z,x}u_{z,y}$ are retained in the Green–Lagrange strain tensor (E_{ij}), the only nonzero components of the von Kármán strain tensor (ε_{ij}) for the Timoshenko beam theory are as follows [8,56]:

$$\varepsilon_{xx} = u^{'} + \frac{1}{2}w^{'2} - z\psi^{'}, \quad \varepsilon_{xz} = \varepsilon_{zx} = \tfrac{1}{2}\left[w^{'} - \psi\right]. \tag{6}$$

Based on the linear elasticity, the nonzero components of the Cauchy force-stress tensor (σ_{ij}) for the micro-/nanobeam can be obtained in terms of displacements as [8,45,57–59]:

$$\begin{cases} \sigma_{xx} = Q^{B}\,(z)\left[u^{'} + \frac{1}{2}w^{'2} - z\psi^{'}\right], \quad Q^{B}\,(z) = 2\mu^{B}\,(z) + \lambda^{B}\,(z)\,, \\ \sigma_{yy} = \sigma_{zz} = \lambda^{B}\,(z)\left[u^{'} + \frac{1}{2}w^{'2} - z\psi^{'}\right], \\ \sigma_{xz} = \sigma_{zx} = k_s\mu^{B}\,(z)\left[w^{'} - \psi\right]. \end{cases} \tag{7}$$

where k_s denotes the shear correction coefficient which accounts for the nonuniformity of the shear strain over the beam cross section [60], i.e., $k_s = 5(1 + \nu_{\mathrm{av}})/(6 + 5\nu_{\mathrm{av}})$, in which the average value of Poisson's ratios of the metal and ceramic phases is $\nu_{\mathrm{av}} = 0.5(\nu_{\mathrm{m}} + \nu_{\mathrm{c}})$. $\mu(z)$ and $\lambda(z)$ are the Lamé constants in the classical elasticity.

According to the modified couple stress theory (MCST) presented by Yang et al. [61] and in light of Eq. (4), the nonzero components of the rotation vector (θ_i), the symmetric curvature tensor (χ_{ij}), and the corresponding deviatoric part of the symmetric couple stress tensor (m_{ij}) can be, respectively, obtained as [8,45,57–59]:

$$\theta_y = -\frac{1}{2}\left[w^{'} + \psi\right], \tag{8}$$

$$\chi_{xy} = \chi_{yx} = -\frac{1}{4}\left[\psi^{'} + w^{''}\right], \tag{9}$$

$$m_{xy} = m_{yx} = -\frac{1}{2}l^{2}\,(z)\,\mu(z)\left[\psi^{'} + w^{''}\right], \tag{10}$$

and $l\,(z)$ refers to the material length scale parameter measuring the couple stress effect.

To this end, the surface energy effects are incorporated into the developed size-dependent model using the Gurtin–Murdoch surface elasticity theory [15,16] in which surface stress–strain relations of the FG Timoshenko nanobeam can be formulated as below [8,20,37],

$$\begin{aligned} \tau_{xx}^{s\pm} &= \tau^{s\pm}\left[1 - \tfrac{1}{2}\,w'^{2}\right] + E^{s\pm}\left[u' - z\psi' + \tfrac{1}{2}w'^{2}\right], \quad E^{s\pm} = 2\mu^{s\pm} + \lambda^{s\pm}, \\ \tau_{xt}^{s\pm} &= \left\{\left(\mu^{s\pm} - \tau^{s\pm}\right)w' - \mu^{s\pm}\psi\right\}n_y \equiv \tau_{xz}^{s\pm}n_y, \\ \tau_{tx}^{s\pm} &= \left\{\mu^{s\pm}w' - \left(\mu^{s\pm} - \tau^{s\pm}\right)\psi\right\}n_y \equiv \tau_{zx}^{s\pm}n_y, \\ \tau_{nx}^{s\pm} &= \tau^{s\pm}u_{n,x} = \tau^{s\pm}n_z w'. \end{aligned} \tag{11}$$

Here, $\tau_{xx}^{s\pm}$, $\tau_{xt}^{s\pm}$, $\tau_{tx}^{s\pm}$, and $\tau_{nx}^{s\pm}$ are the only nonzero components of surface stress, $E^{s\pm}$ denotes the surface elastic modulus, $\mu^{s\pm}$ and $\lambda^{s\pm}$ are the surface Lamé constants, and $\tau^{s\pm}$ is the surface residual stress. The subscript n represents the outward unit normal $\boldsymbol{n}$ to the beam lateral surface, and n_y and n_z represent its y- and z-components, respectively, i.e., $n_y = \cos\theta$ and $n_z = \sin\theta$, where θ is the angle between the normal vector n and the y-axis, as shown in Fig. 1. The subscript t denotes the direction of the unit tangent vector $\boldsymbol{t}$ on the boundary of the beam cross section, i.e., at $\theta = 0$, $\tau_{xz}^{s\pm}$ and $\tau_{zx}^{s\pm}$ are the values of $\tau_{xt}^{s\pm}$and τ_{tx}^{s}, respectively. The indices "+" and "−" represent the upper and lower surfaces of the nanobeam, respectively.

2.3 Size-dependent governing equations

Hamilton's principle is employed to exactly derive the nonlinear size-dependent governing equations and the associated nonclassical boundary conditions (NCBCs):

$$\delta \int_{t1}^{t2} (T - U + W)\,\mathrm{d}t = 0 \tag{12}$$

where U, T, and W are, respectively, the total strain energy, kinetic energy, and work done due to applied external forces.

In the framework of the linear elasticity theory and in accordance with the surface elasticity theory and the modified couple stress theory, the first variation of the total strain energy can be written as [8,56,62]:

$$\begin{aligned}\delta \mathrm{U} &= \frac{1}{2}\delta \int_0^L \int\limits_A \left(\sigma_{ij}\varepsilon_{ij} + m_{ij}\chi_{ij}\right)\mathrm{d}A\mathrm{d}x + \frac{1}{2}\delta \int_0^L \oint_{\partial A} \tau_{ij}^{\mathrm{s}}\varepsilon_{ij}\mathrm{d}S\mathrm{d}x \\ &= \frac{1}{2}\delta \int_0^L \Bigg\{ \int\limits_A \left(\sigma_{xx}\varepsilon_{xx} + 2\sigma_{xz}\varepsilon_{xz} + 2m_{xy}\chi_{xy}\right)\mathrm{d}A \\ &\quad + \oint_{\partial A}\left(\tau_{xx}^{\mathrm{s}}\varepsilon_{xx} + \left(\tau_{xs}^{\mathrm{s}} + \tau_{sx}^{\mathrm{s}}\right)\varepsilon_{xs} + 2\tau_{nx}^{\mathrm{s}}\varepsilon_{nx}\right)\mathrm{d}S\Bigg\}\,\mathrm{d}x\end{aligned} \tag{13}$$

where

$$\varepsilon_{xs} = \varepsilon_{sx} = \frac{1}{2}\left(w' - \psi\right)n_y \equiv \varepsilon_{zx}n_y, \quad \varepsilon_{xn} = \varepsilon_{nx} = \frac{1}{2}w' n_z. \tag{14}$$

Substituting Eqs. (6, 8–11, 14) into Eq. (13) yields

$$\begin{aligned}\delta \int_{t1}^{t2} U\mathrm{d}t = &-\int_{t1}^{t2}\int_0^L \Bigg[\left\{N' + N^{s'} + \frac{1}{2}\mathcal{C}_1 w' w''\right\}\delta u \\ &+ \Bigg\{\frac{1}{2}\left(\mathcal{Q}_1^{s'} + \mathcal{Q}_2^{s'}\right) + \mathcal{Q}_{xz}' + \frac{1}{2}Y_{xy}'' \\ &+ \frac{\mathrm{d}}{\mathrm{d}x}\left(\left[N + N^{\mathrm{s}} + \mathcal{S}_1 - \frac{1}{2}\mathcal{C}_1\left(1 + u'\right) + \frac{1}{2}\mathcal{P}_1\psi'\right]w'\right)\Bigg\}\delta w \\ &+ \left\{-M_x' - \frac{1}{2}Y_{xy}' - M^{s'} + \frac{1}{2}\left(\mathcal{Q}_{s1} + \mathcal{Q}_{s2}\right) + Q_{xz} - \frac{1}{2}\mathcal{P}_1 w' w''\right\}\delta\psi\Bigg]\mathrm{d}x\mathrm{d}t \\ &+ \int_{t1}^{t2}\Bigg[\left\{N + N^{\mathrm{s}} - \frac{1}{2}\mathcal{C}_1\left(1 - \frac{1}{2}w'^2\right)\right\}\delta u \\ &+ \Bigg\{\Bigg\{\frac{1}{2}\left(\mathcal{Q}_1^{\mathrm{s}} + \mathcal{Q}_2^{\mathrm{s}}\right) + Q_{xz} + \frac{1}{2}Y_{xy}' \\ &+ \left(N + N^{\mathrm{s}} + \mathcal{S}_1 - \frac{1}{2}\mathcal{C}_1\left(1 + u'\right) + \frac{1}{2}\mathcal{P}_1\psi'\right)\Bigg\}w'\Bigg\}\delta w \\ &- \left\{\frac{1}{2}Y_{xy}\right\}\delta w' - \left\{M_x + \frac{1}{2}Y_{xy} + M^{\mathrm{s}} - \frac{1}{2}\mathcal{P}_1\left(1 - \frac{1}{2}w'^2\right)\right\}\delta\psi\Bigg]_0^L\mathrm{d}t\end{aligned} \tag{15}$$

in which the stress and couple stress resultants on the beam cross section are expressed as:

$$\left\{\begin{matrix} N \\ M_x \end{matrix}\right\} \equiv \int_A \left\{\begin{matrix} 1 \\ z \end{matrix}\right\}\sigma_{xx}\mathrm{d}A = \left\{\begin{matrix} A_{xx} \\ B_{xx} \end{matrix}\right\}\left[u' + \frac{1}{2}w'^2\right] - \left\{\begin{matrix} B_{xx} \\ D_{xx} \end{matrix}\right\}\psi', \tag{16.1}$$

$$\left\{\begin{matrix} Q_{xz} \\ Y_{xy} \end{matrix}\right\} \equiv \int_A \left\{\begin{matrix} \sigma_{xz} \\ m_{xy} \end{matrix}\right\}\mathrm{d}A = \left\{\begin{matrix} k_s S_{xz}\left[w' - \psi\right] \\ -\frac{1}{2}S_{xy}\left[\psi' + w''\right] \end{matrix}\right\}, \tag{16.2}$$

and the surface stress resultants along the perimeter of the beam cross section are defined as:

$$\left\{\begin{array}{c}N^{\mathrm{s}}\\M^{\mathrm{s}}\end{array}\right\}\equiv\oint_{\partial A}\left\{\begin{array}{c}1\\z\end{array}\right\}\tau_{xx}^{\mathrm{s}}\mathrm{d}S=\left\{\begin{array}{c}\mathcal{C}_1\\\mathcal{P}_1\end{array}\right\}+\left\{\begin{array}{c}\mathcal{C}_2\\\mathcal{P}_2\end{array}\right\}u^{'}+\frac{1}{2}\left\{\begin{array}{c}\mathcal{C}_2-\mathcal{C}_1\\\mathcal{P}_2-\mathcal{P}_1\end{array}\right\}w^{'2}-\left\{\begin{array}{c}\mathcal{P}_2\\I_{\mathrm{P}}\end{array}\right\}\psi^{'}, \tag{16.3}$$

$$\left\{\begin{array}{c}\mathcal{Q}_1^{\mathrm{s}}\\\mathcal{Q}_2^{\mathrm{s}}\end{array}\right\}\equiv\oint_{\partial A}n_y^2\left\{\begin{array}{c}\tau_{xz}^{\mathrm{s}}\\\tau_{zx}^{\mathrm{s}}\end{array}\right\}\mathrm{d}S=\left\{\begin{array}{c}\mathcal{L}_2-\mathcal{L}_1\\\mathcal{L}_2\end{array}\right\}w^{'}-\left\{\begin{array}{c}\mathcal{L}_2\\\mathcal{L}_2-\mathcal{L}_1\end{array}\right\}\psi \tag{16.4}$$

in which

$$\left\{A_{xx}\ B_{xx}\ D_{xx}\ S_{xz}\ S_{xy}\right\}=\int\limits_A\left\{Q^B(z)\ zQ^B(z)\ z^2Q^B(z)\ \mu^B(z)\ l(z)^2\,\mu^B(z)\right\}\mathrm{d}A \tag{17.1}$$

$$\begin{aligned}&\left\{\mathcal{C}_1\ \mathcal{C}_2\ \mathcal{P}_1\ \mathcal{P}_2\ \mathcal{S}_1\ I_{\mathrm{P}}\ \mathcal{L}_1\ \mathcal{L}_2\right\}\\&=\oint_{\partial A}\left\{\tau^{\mathrm{s}}(z)\ E^{\mathrm{s}}(z)\ z\tau^{\mathrm{s}}(z)\ zE^{\mathrm{s}}(z)\ n_z^2\tau^{\mathrm{s}}(z)\ z^2E^{\mathrm{s}}(z)\ n_y^2\tau^{\mathrm{s}}(z)\ n_y^2\mu^{\mathrm{s}}(z)\right\}\mathrm{d}S.\end{aligned} \tag{17.2}$$

The first variation of the kinetic energy of the FGM Timoshenko nanobeam accounting for the surface density effect can be written in terms of displacements as:

$$\begin{aligned}\delta\int_{t1}^{t2}\mathrm{T}&=\int_{t1}^{t2}\frac{1}{2}\delta\int_0^L\left\{\int_A\rho^B(z)\left(\dot{u}_x^2+\dot{u}_y^2+\dot{u}_z^2\right)\mathrm{d}A+\oint_{\partial A}\rho^{\mathrm{s}}(z)\left(\dot{u}_x^2+\dot{u}_y^2+\dot{u}_z^2\right)\mathrm{d}S\right\}\mathrm{d}x\mathrm{d}t\\&=\int_{t1}^{t2}\left[\int_0^L\left\{\left[I_0\dot{u}-I_1\dot{\psi}\right]\delta\dot{u}-\left[I_1\dot{u}-I_2\dot{\psi}\right]\delta\dot{\psi}+I_0\dot{w}\delta\dot{w}\right\}\mathrm{d}x\right]\mathrm{d}t\end{aligned} \tag{18}$$

where the mass inertia coefficients (I_0, I_1, and I_2) including the effect of surface density are defined by:

$$\left\{I_0\ I_1\ I_2\right\}=\int_A\left\{\rho^B(z)\ z\rho^B(z)\ z^2\rho^B(z)\right\}\mathrm{d}A+\oint_{\partial A}\left\{\rho^{\mathrm{s}}(z)\ z\rho^{\mathrm{s}}(z)\ z^2\rho^{\mathrm{s}}(z)\right\}\mathrm{d}S. \tag{19}$$

Additionally, the variational form of the work done by the external forces applied on the FG nanobeam is given by:

$$\begin{aligned}\delta\int_{t1}^{t2}W\mathrm{d}t&=\int_{t1}^{t2}\left[\int_0^L\left[q\delta w+f_{\mathrm{c}}\delta\theta_y\right]\mathrm{d}x\right]\mathrm{d}t+\int_{t1}^{t2}\left[\bar{N}\delta u+\bar{V}\delta w+\bar{M}_{\mathrm{m}}\delta w^{'}+\bar{M}_{\sigma}\delta\psi\right]_0^L\mathrm{d}t\\&=\int_{t1}^{t2}\int_0^L\left[\left(q+\frac{1}{2}f_{\mathrm{c}}^{'}\right)\delta w-\frac{1}{2}f_{\mathrm{c}}\delta\psi\right]\mathrm{d}x\mathrm{d}t\\&\quad+\int_{t1}^{t2}\left[\bar{N}\delta u+\left(\bar{V}-\frac{1}{2}f_{\mathrm{c}}\right)\delta w+\bar{M}_{\mathrm{m}}\delta w^{'}+\bar{M}_{\sigma}\delta\psi\right]_0^L\mathrm{d}t\end{aligned} \tag{20}$$

where q is the z-component of body force per unit length along the x-axis and f_{c} is the y-component of the body couple imposed on the sections as couple per unit axial length (per unit volume along the x-axis). $\bar{N}$, $\bar{V}$, $\bar{M}_{\sigma}$, and $\bar{M}_{\mathrm{m}}$ denote, respectively, the applied axial resultant force of normal stresses, the transverse resultant force of shear stresses, the resultant external bending moment of normal stresses, and the resultant external bending moment around the y-axis due to couple stresses at the beam ends.

Substituting Eqs. (15, 18, 20) into Eq. (12), applying the fundamental lemma of calculus of variations, and gathering the coefficients of δu, δw, and $\delta\psi$, the nonlinear nonclassical governing differential equations of motion of a FG Timoshenko nanobeam can be achieved as:

$$\delta u\colon I_1\ddot{\psi}-I_0\ddot{u}+N^{'}+N^{s^{'}}+\frac{1}{2}\mathcal{C}_1w^{'}w^{''}=0, \tag{21.1}$$

$$\begin{aligned}&\delta w\colon -I_0\ddot{w}+\frac{1}{2}\left(\mathcal{Q}_1^{s^{'}}+\mathcal{Q}_2^{s^{'}}\right)+\mathcal{Q}_{xz}^{'}+\frac{1}{2}Y_{xy}^{''}+\left(N^{'}+N^{s^{'}}-\frac{1}{2}\mathcal{C}_1u^{''}+\frac{1}{2}\mathcal{P}_1\psi^{''}\right)w^{'}\\&\quad+\left(N+N^{\mathrm{s}}+\mathcal{S}_1-\frac{1}{2}\mathcal{C}_1\left(1+u^{'}\right)+\frac{1}{2}\mathcal{P}_1\psi^{'}\right)w^{''}+\left(q+\frac{1}{2}f_{\mathrm{c}}^{'}\right)=0,\end{aligned} \tag{21.2}$$

$$\delta\psi\colon I_1\ddot{u}-I_2\ddot{\psi}-M_x^{'}-\frac{1}{2}Y_{xy}^{'}-M^{s^{'}}+\frac{1}{2}\left(\mathcal{Q}_1^{\mathrm{s}}+\mathcal{Q}_2^{\mathrm{s}}\right)+Q_{xz}-\frac{1}{2}\mathcal{P}_1w^{'}w^{''}-\frac{1}{2}f_{\mathrm{c}}=0. \tag{21.3}$$

Moreover, the associated nonclassical boundary conditions (NCBCs) at the beam ends ($x = 0, L$) can be expressed as:

$$\delta u\text{: either} \quad u = \bar{u} \quad \text{or} \quad N + N^{\mathrm{s}} - \frac{1}{2}\mathcal{C}_1\left(1 - \frac{1}{2}w^{'2}\right) - \bar{N} = 0, \tag{22.1}$$

$$\delta w\text{: either} \quad w = \bar{w} \quad \text{or} \quad \frac{1}{2}\left(\mathcal{Q}_1^{\mathrm{s}} + \mathcal{Q}_2^{\mathrm{s}}\right) + Q_{xz} + \frac{1}{2}Y_{xy}^{'}$$
$$+ \left(\mathcal{S}_1 + N + N^{\mathrm{s}} - \frac{1}{2}\mathcal{C}_1\left(1 + u^{'}\right) + \frac{1}{2}\mathcal{P}_1\psi^{'}\right)w^{'} + \frac{1}{2}f_{\mathrm{c}} - \bar{V} = 0, \tag{22.2}$$

$$\delta\psi\text{: either} \quad \psi = \bar{\psi} \quad \text{or} \quad M_x + \frac{1}{2}Y_{xy} + M^{\mathrm{s}} - \frac{1}{2}\mathcal{P}_1\left(1 - \frac{1}{2}w^{'2}\right) + \bar{M}_\sigma = 0, \tag{22.3}$$

$$\delta w^{'}\text{: either} \quad w^{'} = \bar{w}^{'} \quad \text{or} \quad \frac{1}{2}Y_{xy} + \bar{M}_{\mathrm{m}} = 0. \tag{22.4}$$

By inserting the force and moment resultants introduced in Eq. (16.1) into Eqs. (21.1) and (22.1), the size-dependent nonlinear governing equations and the corresponding NCBCs in terms of displacement components can be, respectively, obtained as:

$$I_1\ddot{\psi} - I_0\ddot{u} + A_{11}u^{''} - B_{11}\psi^{''} + A_{22}w^{'}w^{''} = 0, \tag{23.1}$$

$$-I_0\ddot{w} + \left[\mathrm{S}_{11} + \mathcal{S}_1 + \frac{1}{2}\mathcal{C}_1 + A_{22}u^{'} + \frac{3}{2}A_{33}w^{'2} - B_{22}\psi^{'}\right]w^{''} - \frac{1}{4}S_{xy}w^{''''}$$
$$-\frac{1}{4}S_{xy}\psi^{'''} - \mathrm{S}_{11}\psi^{'} + \left[A_{22}u^{''} - B_{22}\psi^{''}\right]w^{'} + q + \frac{1}{2}f_{\mathrm{c}}^{'} = 0, \tag{23.2}$$

$$I_1\ddot{u} - I_2\ddot{\psi} - B_{11}u^{''} + \frac{1}{4}S_{xy}w^{'''} + \mathrm{S}_{11}w^{'} + D_{11}\psi^{''} - \mathrm{S}_{11}\psi - B_{22}w^{'}w^{''} - \frac{1}{2}f_{\mathrm{c}} = 0, \tag{23.3}$$

and

$$u = \bar{u} \quad \text{or} \quad A_{11}u^{'} - B_{11}\psi^{'} + \frac{1}{2}A_{22}w^{'2} - \bar{N} + \frac{1}{2}\mathcal{C}_1 = 0, \tag{24.1}$$

$$w = \bar{w} \quad \text{or} \quad -\frac{1}{4}S_{xy}w^{'''} - S_{11}\psi - \frac{1}{4}S_{xy}\psi^{''}$$
$$+\left[S_{11} + \mathcal{S}_1 + \frac{1}{2}\mathcal{C}_1 + A_{22}u^{'} + \frac{1}{2}A_{22}w^{'2} - B_{22}\psi^{'}\right]w^{'} + \frac{1}{2}f_{\mathrm{c}} - \bar{V} = 0, \tag{24.2}$$

$$\psi = \bar{\psi} \text{or} \quad B_{11}u^{'} - \frac{1}{4}S_{xy}w^{''} - D_{11}\psi^{'} + \frac{1}{2}B_{22}w^{'2} + \frac{1}{2}\mathcal{P}_1 + \bar{M}_\sigma = 0, \tag{24.3}$$

$$w^{'} = \bar{w}^{'} \text{or} \quad \frac{1}{4}S_{xy}\left(\psi^{'} + w^{''}\right) - \bar{M}_{\mathrm{m}} = 0 \tag{24.4}$$

where

$$\left\{D_{11} \;\; S_{11}\right\} = \left\{\left(\frac{S_{xy}}{4} + D_{xx} + I_{\mathrm{P}}\right)\left(k_s S_{xz} + \mathcal{L}_2 - \frac{\mathcal{L}_1}{2}\right)\right\}, \tag{25.1}$$

$$\left\{A_{11} \;\; A_{22} \;\; A_{33} \;\; B_{11} \;\; B_{22}\right\} = \left\{(A_{xx} + \mathcal{C}_2)\left(A_{11} - \frac{\mathcal{C}_1}{2}\right)(A_{11} - \mathcal{C}_1)\,(B_{xx} + \mathcal{P}_2)\left(B_{11} - \frac{\mathcal{P}_1}{2}\right)\right\}. \tag{25.2}$$

Up to here, a nonlinear nonclassical functionally graded Timoshenko nanobeam model is developed incorporating the simultaneous effect of microstructure, surface elasticity, surface mass density, surface residual stress, and von Kármán geometric nonlinearity. It is important to mention that the linear equations of motion of a homogeneous Timoshenko nanobeam with the effects of surface energy and modified coupled stress derived by Gao [22] can be recovered from Eq. (23) by dropping the nonlinear terms and setting the gradient index $k = 0$. Further, the homogeneous Timoshenko nanobeam model developed by Ansari et al. [18] considering the surface energy effect and von Kármán geometric nonlinearity can be recovered from the present model by setting $k = l = 0$, as there are some missed terms in their variation of surface strain energy.

2.4 Dimensionless size-dependent governing equations

We introduce the following dimensionless parameters:

$$\left\{ x^* \; u^* \; w^* \; \psi^* \; t^* \; \Omega \right\} = \left\{ \tfrac{x}{L} \; \tfrac{u}{h} \; \tfrac{w}{h} \; \psi \; \tfrac{t}{\tau} \; \tau\omega \right\}, \quad \tau = L^2\sqrt{\frac{\rho_{\mathrm{m}} A_0}{E_{\mathrm{m}} I_{\mathrm{m}}}} \tag{26}$$

where $A_0 = bh$, $I_{\mathrm{m}} = (bh^3)/12$. Using Eq. (26) and letting $\xi = L/h$, the nondimensional governing equations for nonlinear free vibration, where all the external forces vanish in Eqs. (23.1) and (24.1), can be obtained as:

$$I_1^*\ddot{\psi} - I_0^*\ddot{u} + \xi^2 A_{11}^* u'' - \xi^2 B_{11}^* \psi'' + \xi A_{22}^* w' w'' = 0, \tag{27.1}$$

$$-I_0^*\ddot{w} + \xi^2\left(S_{11}^* + \mathcal{S}_1^* + \frac{1}{2}\mathcal{C}_1^*\right) w'' - \frac{1}{4} S_{xy}^* w'''' - \frac{1}{4}\xi S_{xy}^* \psi''' - \xi^3 S_{11}^* \psi' + \xi A_{22}^* \left[u'' w' + u' w''\right]$$
$$-\xi B_{22}^* \left[\psi'' w' + \psi' w''\right] + \frac{3}{2} A_{33}^* w'^2 w'' = 0, \tag{27.2}$$

$$I_1^*\ddot{u} - I_2^*\ddot{\psi} - \xi^2 B_{11}^* u'' + \xi^3 S_{11}^* w' + \frac{1}{4}\xi S_{xy}^* w''' - \xi^4 S_{11}^* \psi + \xi^2 D_{11}^* \psi'' - \xi B_{22}^* w' w'' = 0. \tag{27.3}$$

(a) *Simply supported end support*

$$\begin{cases} \frac{A_{11}^*}{\xi} u' - \frac{B_{11}^*}{\xi} \psi' + \frac{1}{2}\frac{A_{22}^*}{\xi^2} w'^2 + \frac{1}{2}\mathcal{C}_1^* = 0, \\ w = 0, \\ \frac{B_{11}^*}{\xi} u' - \frac{1}{4}\frac{S_{xy}^*}{\xi^2} w'' - \frac{D_{11}^*}{\xi} \psi' + \frac{1}{2}\frac{B_{22}^*}{\xi^2} w'^2 + \frac{1}{2}\mathcal{P}_1^* = 0, \\ \frac{1}{\xi} w'' + \psi' = 0. \end{cases} \tag{28.1}$$

(b) *Clamped end support*

$$u = w = 0, \quad \psi = 0, w' = 0 \tag{28.2}$$

with

$$\begin{cases} \left\{ I_0^* \; I_1^* \; I_2^* \right\} = \frac{1}{\rho_{\mathrm{m}} A_0} \left\{ I_0 \; \frac{I_1}{h} \; \frac{I_2}{h^2} \right\}, \\ \left\{ A_{11}^* \; A_{22}^* \; A_{33}^* \; B_{11}^* \; B_{22}^* \right\} = \frac{h}{E_{\mathrm{m}} I_{\mathrm{m}}} \left\{ hA_{11} \; hA_{22} \; hA_{33} \; B_{11} \; B_{22} \right\}, \\ \left\{ S_{xy}^* \; S_{11}^* \; D_{11}^* \; \mathcal{S}_1^* \; \mathcal{C}_1^* \; \mathcal{P}_1^* \right\} = \frac{1}{E_{\mathrm{m}} I_{\mathrm{m}}} \left\{ S_{xy} \; h^2 S_{11} \; D_{11} \; h^2 \mathcal{S}_1 \; h^2 \mathcal{S}_1 \; h\mathcal{P}_1 \right\}. \end{cases} \tag{29}$$

After some mathematical manipulation, the explicit representation of the system given by Eq. (27.1) is as follows:

$$\mathbb{k}_1 \ddot{u} + \mathbb{k}_2 u'' + \mathbb{k}_3 \psi'' + \mathbb{k}_4 w' w'' + \mathbb{k}_5 w' + \mathbb{k}_6 w''' + \mathbb{k}_7 \psi = 0, \tag{30.1}$$

$$\mathbb{I}_{\mathrm{w}} \ddot{w} + \mathbb{c}_0 w'' + \mathbb{c}_1 w'''' + \mathbb{c}_2 \psi'''$$
$$+\mathbb{c}_3 \psi' + \mathbb{c}_4 \left[u'' w' + u' w''\right] + \mathbb{c}_5 \left[\psi'' w' + \psi' w''\right] + \mathbb{c}_6 w'^2 w'' = 0, \tag{30.2}$$

$$\mathbb{p}_1 \ddot{\psi} + \mathbb{p}_2 \psi'' + \mathbb{p}_3 u'' + \mathbb{p}_4 w' w'' + \mathbb{p}_5 w' + \mathbb{p}_6 w''' + \mathbb{p}_7 \psi = 0 \tag{30.3}$$

in which

$$\begin{Bmatrix} \mathbb{k}_1 \\ \mathbb{k}_2 \\ \mathbb{k}_3 \\ \mathbb{k}_4 \\ \mathbb{k}_5 \\ \mathbb{k}_6 \\ \mathbb{k}_7 \end{Bmatrix} = \begin{Bmatrix} -I_0^* + r_1 I_1^* \\ \xi^2 \left(A_{11}^* - r_1 B_{11}^*\right) \\ -\xi^2 \left(B_{11}^* + r_1 D_{11}^*\right) \\ \xi \left(A_{22}^* - r_1 B_{22}^*\right) \\ \xi^3 r_1 S_{11}^* \\ \frac{\xi r_1 S_{xy}^*}{4} \\ -\xi^4 r_1 S_{11}^* \end{Bmatrix},$$

$$\begin{Bmatrix} \mathbb{p}_1 \\ \mathbb{p}_2 \\ \mathbb{p}_3 \\ \mathbb{p}_4 \\ \mathbb{p}_5 \\ \mathbb{p}_6 \\ \mathbb{p}_7 \end{Bmatrix} = \begin{Bmatrix} -I_2^* + r_2 I_1^* \\ \xi^2 \left(D_{11}^* - r_2 B_{11}^*\right) \\ -\xi^2 \left(B_{11}^* + r_2 A_{11}^*\right) \\ -\xi \left(B_{22}^* + r_2 A_{22}^*\right) \\ \xi^3 S_{11}^* \\ \xi S_{xy}^*/4 \\ -\xi^4 S_{11}^* \end{Bmatrix},$$

$$\begin{Bmatrix} \mathbb{c}_0 \\ \mathbb{c}_1 \\ \mathbb{c}_2 \\ \mathbb{c}_3 \\ \mathbb{c}_4 \\ \mathbb{c}_5 \\ \mathbb{c}_6 \end{Bmatrix} = \begin{Bmatrix} \xi^2 \left(S_{11}^* + \mathcal{S}_1^* + \frac{1}{2}\mathcal{C}_1^*\right) \\ -S_{xy}^*/4 \\ -\xi S_{xy}^*/4 \\ -\xi^3 S_{11}^* \\ \xi A_{22}^* \\ -\xi B_{22}^* \\ 3A_{33}^*/2 \end{Bmatrix}, \quad \begin{Bmatrix} r_1 \\ r_2 \\ \mathbb{I}_w \end{Bmatrix} = -\begin{Bmatrix} \frac{I_1^*}{I_2^*} \\ \frac{I_1^*}{I_0^*} \\ I_0^* \end{Bmatrix}. \tag{31}$$

It is important to notice that, compared with the clamped end boundary conditions, the simply supported boundary conditions given by Eq. (28.1) are not only nonlinear but also nonhomogeneous (nonideal) due to the presence of the terms $\mathcal{P}_1^*/2$ and $C_1^*/2$. These terms are nonzero when including the effect of the surface residual stress of the FG nanobeam, i.e., when $\tau_s \neq 0$ and $k \neq 0$ as seen from Eq. (17.2). Some recent works [20, 25, 26, 37] have studied FG nanostructures including surface effects and derived the mathematical models with similar nonhomogeneous boundary conditions. However, they solved these models analytically and applied the classical boundary conditions rather than the exact nonhomogeneous ones. In fact, these nonclassical (nonhomogeneous) terms act as self-excitation loading and cause deformation of the microstructure at no external load.

3 Solution strategy

In the present study, the nonlinear governing equations are solved employing the GDQM as one of the most efficient numerical techniques.

3.1 Discretization in *x*-direction using GDQM

The normalized beam length $0 \leq x \leq 1$ is discretized to n points: $x_1 = 0$, $x_2 = \delta$, $x_{n-1} = 1 - \delta$, $x_n = 1$, and the other inner nodes x_i are calculated using the Chebyshev–Gauss–Lobatto formula:

$$x_i = \frac{1}{2}\left(1 - \cos\frac{(i-2)\pi}{n-3}\right) i = 3, 4, \ldots, n-2. \tag{32}$$

Here, δ is a small number and is taken in this study as $\delta = 0.04x_3$.

GDQM is a polynomial-based discretization method that approximates derivatives of a function $v(x)$ as a weighted sum of its values at all discrete nodes in its domain. For a vector $V = [v_1, v_2, \ldots, v_n]^{\mathrm{T}}$ of nodal values of $v(x)$, i.e.,$v_i = v(x_i)$, the first-order nodal derivative vector $V^{'} = \left[v_1^{'}, v_2^{'}, \ldots, v_n^{'}\right]^{\mathrm{T}}, v_i^{'} = \frac{\mathrm{d}v}{\mathrm{d}x}\Big|_{x_i}$ can be computed as $V^{'} = \mathcal{A}V$, where $\mathcal{A}$ is the first-order derivative weighting coefficient matrix of dimension $n \times n$ and is computed as [63],

$$\mathcal{A}_{ij} = \begin{cases} \frac{1}{x_i - x_j} \prod\limits_{\substack{m=1 \\ m \neq i, m \neq j}}^{n} \frac{x_i - x_{\mathrm{m}}}{x_j - x_{\mathrm{m}}}, & i \neq j \\ \sum\limits_{\substack{m \neq i \\ m=1}}^{n} \frac{1}{x_{\mathrm{m}} - x_i}, & i = j. \end{cases} \tag{33}$$

Based on the GDQM, the unknown functions $w\,(x)$, $u(x)$, and $\psi(x)$ in Eq. (30) are discretized to three vectors W, U, and Ψ where $W = [w_1, w_2, \ldots, w_n]^{\mathrm{T}}$, $U = [u_1, u_2, \ldots, u_n]^{\mathrm{T}}$, and $\Psi = [\psi_1, \psi_2, \ldots, \psi_n]^{\mathrm{T}}$. The associated derivative vectors are approximated as:

$$\begin{gathered} \begin{Bmatrix} W' \\ W'' \\ W''' \\ W'''' \end{Bmatrix} = \begin{Bmatrix} \mathcal{A} \\ \mathcal{B} \\ \mathcal{C} \\ \mathcal{D} \end{Bmatrix} W, \\ \begin{Bmatrix} U' \\ U'' \\ U''' \end{Bmatrix} = \begin{Bmatrix} \mathcal{A} \\ \mathcal{B} \\ \mathcal{C} \end{Bmatrix} U, \begin{Bmatrix} \Psi' \\ \Psi'' \\ \Psi''' \end{Bmatrix} = \begin{Bmatrix} \mathcal{A} \\ \mathcal{B} \\ \mathcal{C} \end{Bmatrix} \Psi \end{gathered} \tag{34}$$

where $\mathcal{B} = \mathcal{A}\mathcal{A}$, $\mathcal{C} = \mathcal{A}\mathcal{B}$, and $\mathcal{D} = \mathcal{A}\mathcal{C}$.

3.2 Nonlinear vibration of an FG Timoshenko nanobeam

The difficulty encountered in the nonhomogeneous nonlinear boundary conditions (Eq. 28.2) is the fact that in the Galerkin's approach the solution of a dynamic system is assumed to be a finite sum of products of two functions in space and time variables. The space functions must satisfy the boundary conditions that necessarily should be homogeneous. In order to effectively handle such nonhomogeneous nonlinear boundary conditions, the solution is assumed to consist of two parts, as shown in Eq. (35). The first part is the static solution $\{w_s, u_s, \psi_s\}$, in which the nonhomogeneous boundary conditions are considered during its evaluation. The second part is the dynamic solution $\{w_d, u_d, \psi_d\}$

$$\begin{aligned} w\,(x,t) &= w_s\,(x) + w_d(x,t), \\ u\,(x,t) &= u_s\,(x) + u_d(x,t), \\ \psi\,(x,t) &= \psi_s\,(x) + \psi_d(x,t). \end{aligned} \tag{35}$$

3.2.1 Static solution

Dropping the inertia and time-dependent terms in Eq. (30) and substituting Eq. (35), the governing equation for the static response of FG Timoshenko nanobeam can be achieved as:

$$\mathbb{k}_2 u_s^{''} + \mathbb{k}_3 \psi_s^{''} + \mathbb{k}_4 w_s^{'} w_s^{''} + \mathbb{k}_5 w_s^{'} + \mathbb{k}_6 w_s^{'''} + \mathbb{k}_7 \psi_s = 0, \tag{36.1}$$

$$\mathbb{c}_0 w_s^{''} + \mathbb{c}_1 w_s^{''''} + \mathbb{c}_2 \psi_s^{'''} + \mathbb{c}_3 \psi_s^{'} + \mathbb{c}_4 \left[u_s^{''} w_s^{'} + u_s^{'} w_s^{''}\right] + \mathbb{c}_5 \left[\psi_s^{''} w_s^{'} + \psi_s^{'} w_s^{''}\right] + \mathbb{c}_6 w_s^{'2} w_s^{''} = 0, \tag{36.2}$$

$$\mathbb{p}_2 \psi_s^{''} + \mathbb{p}_3 u_s^{''} + \mathbb{p}_4 w_s^{'} w_s^{''} + \mathbb{p}_5 w_s^{'} + \mathbb{p}_6 w_s^{'''} + \mathbb{p}_7 \psi_s = 0, \tag{36.3}$$

and the following nonhomogeneous boundary conditions of a simply supported nanobeam:

$$\begin{cases} \frac{A_{11}^*}{\xi} u_s^{'} - \frac{B_{11}^*}{\xi} \psi_s^{'} + \frac{1}{2} \frac{A_{22}^*}{\xi^2} \; w_s^{'2} + \frac{1}{2} \mathcal{C}_1^* = 0, \\ w_s = 0, \\ \frac{B_{11}^*}{\xi} u_s^{'} - \frac{1}{4} \frac{S_{xy}^*}{\xi^2} w_s^{''} - \frac{D_{11}^*}{\xi} \psi_s^{'} + \frac{1}{2} \frac{B_{22}^*}{\xi^2} \; w_s^{'2} + \frac{1}{2} \mathcal{P}_1^* = 0, \\ \frac{1}{\xi} w_s^{''} + \psi_s^{'} = 0. \end{cases} \tag{37}$$

Discretization of the governing nonlinear system, Eq. (36), and the nonlinear nonclassical boundary conditions, Eq. (37), by the GDQM result in a nonlinear system of algebraic equations. The Newton method is implemented to approximate the static response $\{w_s, u_s, \psi_s\}$ of the nonlinear system. To improve accuracy and run time, the Jacobian matrix is derived analytically. For more details, refer to the recent work of Shanab et al. [8]

3.2.2 Dynamic solution

By inserting Eq. (35) into the nonlinear system (Eq. 30) and making use of Eq. (36), the nonlinear system of PDEs in the time-dependent variables $w_d(x, t)$, $u_d(x, t)$, and $\psi_d(x, t)$ that describe the dynamic response of an FG Timoshenko nanobeam is obtained as:

$$\mathbb{k}_1 \ddot{u}_d + \mathbb{k}_2 u_d^{''} + \mathbb{k}_3 \psi_d^{''} + \mathbb{k}_4 \left(w_s^{'} w_d^{''} + w_s^{''} w_d^{'} + w_d^{'} w_d^{''} \right) + \mathbb{k}_5 w_d^{'} + \mathbb{k}_6 w_d^{'''} + \mathbb{k}_7 \psi_d = 0, \tag{38.1}$$

$$\begin{aligned} &\mathbb{I}_w \ddot{w}_d + \mathbb{c}_0 w_d^{''} + \mathbb{c}_1 w_d^{''''} + \mathbb{c}_2 \psi_d^{'''} + \mathbb{c}_3 \psi_d^{'} + \mathbb{c}_4 \left[u_s^{''} w_d^{'} + w_s^{'} u_d^{''} + u_s^{'} w_d^{''} + w_s^{''} u_d^{'} + w_d^{'} u_d^{''} + w_d^{''} u_d^{'} \right], \\ &\quad + \mathbb{c}_5 \left[\psi_s^{''} w_d^{'} + w_s^{'} \psi_d^{''} + \psi_s^{'} w_d^{'} + w_s^{''} \psi_d^{'} + w_d^{'} \psi_d^{''} + w_d^{''} \psi_d^{'} \right] \\ &\quad + \mathbb{c}_6 \left(w_s^{'2} w_d^{''} + 2 w_s^{'} w_s^{''} w_d^{'} + 2 w_s^{'} w_d^{'} w_d^{''} + w_s^{''} w_d^{'2} + w_d^{''} w_d^{'2} \right) = 0, \end{aligned} \tag{38.2}$$

$$\mathbb{p}_1 \ddot{\psi}_d + \mathbb{p}_2 \psi_d^{''} + \mathbb{p}_3 u_d^{''} + \mathbb{p}_4 \left(w_s^{'} w_d^{''} + w_s^{''} w_d^{'} + w_d^{'} w_d^{''} \right) + \mathbb{p}_5 w_d^{'} + \mathbb{p}_6 w_d^{'''} + \mathbb{p}_7 \psi_d = 0. \tag{38.3}$$

Similarly, by substituting Eq. (35) into Eq. (28.1) and making use of Eq. (37), the nonlinear boundary conditions at the simply supported end can be obtained as:

$$\begin{cases} \frac{A_{11}^*}{\xi} u_d^{'} - \frac{B_{11}^*}{\xi} \psi_d^{'} + \frac{1}{2} \frac{A_{22}^*}{\xi^2} \; \left(2 w_s^{'} w_d^{'} + w_d^{'2} \right) = 0, \\ w_d = 0, \\ \frac{B_{11}^*}{\xi} u_d^{'} - \frac{1}{4} \frac{S_{xy}^*}{\xi^2} w_d^{''} - \frac{D_{11}^*}{\xi} \psi_d^{'} + \frac{1}{2} \frac{B_{22}^*}{\xi^2} \; \left(2 w_s^{'} w_d^{'} + w_d^{'2} \right) = 0, \\ \frac{1}{\xi} w_d^{''} + \psi_d^{'} = 0. \end{cases} \tag{39}$$

3.3 Fundamental nonlinear frequency

For the nonlinear free vibration analysis, the single-mode and multi-mode Galerkin's method can be used to convert Eq. (38) to a system of nonlinear ordinary differential equations. At low amplitude ratios, it is found that the number of modes has a minor effect on the nonlinear frequency ratios of nanobeams [64]. Thus, the single-mode Galerkin's method can provide the nonlinear frequency of nanobeams with good accuracy. Here, the nonlinear dynamics of an FG Timoshenko nanobeam is studied to get the nonlinear free vibration frequency Ω_{NL} using the single-mode Galerkin method, such that

$$\begin{Bmatrix} w_d(x, t) \\ u_d(x, t) \\ \psi_d(x, t) \end{Bmatrix} = \begin{Bmatrix} \phi_w(x) q_w(t) \\ \phi_u(x) q_u(t) \\ \phi_\psi(x) q_\psi(t) \end{Bmatrix} \tag{40}$$

where $q_w(t)$, $q_u(t)$, and $q_\psi(t)$ are the time response of the beam corresponding to w, u, and ψ, respectively. The spatial functions $\phi_w(x)$, $\phi_u(x)$, and $\phi_\psi(x)$ represent the linear first-mode shapes corresponding to w, u, and ψ, respectively. These mode shapes are the eigenvectors of the linear eigenvalue problem, which results from discretizing the linear problem obtained after dropping the nonlinear terms in Eqs. (38) and (39).

Substituting Eq. (40) into Eq. (38), multiplying the resulting equations from Eqs. (38.1), (38.2), and (38.3) by ϕ_u, ϕ_w, and ϕ_ψ, respectively, then integrating with respect to x from 0 to 1, the following system of three nonlinear differential equations can be obtained:

$$\mathbb{K}_1\ddot{q}_u + \mathbb{K}_2 q_u + \mathbb{K}_3 q_w + \mathbb{K}_4 q_\psi + \mathbb{K}_5 q_w^2 = 0, \tag{41.1}$$

$$\mathbb{M}_1\ddot{q}_w + \mathbb{M}_2 q_w + \mathbb{M}_3 q_\psi + \mathbb{M}_4 q_u + \mathbb{M}_5 q_u q_w + \mathbb{M}_6 q_\psi q_w + \mathbb{M}_7 q_w^2 + \mathbb{M}_8 q_w^3 = 0, \tag{41.2}$$

$$\mathbb{P}_1\ddot{q}_\psi + \mathbb{P}_2 q_\psi + \mathbb{P}_3 q_u + \mathbb{P}_4 q_w + \mathbb{P}_5 q_w^2 = 0. \tag{41.3}$$

The coefficients of Eq. (41) are provided in "Appendix A". The nonlinear system of ordinary differential equations Eq. (41) is solved using two different techniques. The first one is the Runge–Kutta method, which is preferred to study the transient response of the problem. However, the steady-state nonlinear frequency can be calculated from the three responses $q_w(t)$, $q_u(t)$, and $q_\psi(t)$ obtained after a sufficiently long time. It is found that the three responses oscillate with the same frequency. The other technique composes discretizing the differential equations in Eq. (41) by a spectral collocation method [65]; then, the solution is obtained using the pseudo-arclength continuation method [66]; see "Appendix B". The later technique is more suitable to study the steady-state response of the problem under consideration, determine the nonlinear frequency, and obtain the frequency–response relationship.

4 Model verification

First of all, let us verify the accuracy of the present model and convergence of the solution procedures by comparing the degenerated results with those reported in the available open literature. For the purpose of comparison with results based on the Euler–Bernoulli beam theory (EBBT), the present TBT model is reduced to the EBBT model by replacing the rotation of the beam cross section ψ in Eq. (4) with w'. On the other hand, the comparison with the classical beam theory is obtained from the developed model by setting all nonclassical parameters related to couple stress and surface energy equal to zero (i.e., $\tau^s = E^s = \rho^s = l = 0$). In addition, results for a homogeneous beam are produced from the present model by setting the gradient index equal to zero (i.e., $k = 0$).

4.1 Comparison with the available literature

In Table 1, the first three fundamental linear frequencies of simply–simply supported (SS) and clamped–clamped (CC) homogeneous micro-/nanobeams based on EBBT and the classical analysis are validated with the results obtained in [67,68]. Additionally, the convergence of GDQM is also investigated using different grid points n. It is observed that only nine grid points are sufficient for the convergence of GDQM in this case. Based on the classical theory and EBBT, the dimensionless linear frequencies of a simply supported power law and sigmoid FGM beam are summarized in Tables 2 and 3, respectively. The results are compared with the available literature [20,69–71], and good agreement is found. Based on the fully nonclassical (with the simultaneous effect of surface energy and couple stress) and classical analyses, the fundamental linear

Table 1 Convergence and validation of GDQM for the dimensionless fundamental linear frequencies of simply supported and clamped–clamped homogeneous beams based on the classical analysis of EBBT ($L = 10$, $L/h = 20$, $b = h$, $E = 30\,\text{MPa}$, $\rho = 1$, $\nu = 0.24$)

Solution method	Number of grid points (n)	Simply supported			Clamped–clamped		
		Mode 1	Mode 2	Mode 3	Mode 1	Mode 2	Mode 3
Present GDQM	7	9.8348	45.5596	83.0232	22.3420	62.3166	111.3495
	9	9.8595	39.3674	84.5483	22.3447	61.3849	118.9361
	11	9.8595	39.3181	87.9463	22.3447	61.3791	119.6679
	15	9.8595	39.3171	88.0158	22.3447	61.3790	119.6766
	21	9.8595	39.3171	88.0158	22.3447	61.3790	119.6766
Mohamed et al. [67]		9.8595	39.3171	88.0158	22.3447	61.3790	119.6760
Reddy [68]		9.8600	39.3200	88.0200	–	–	–

Table 2 Comparison of dimensionless linear classical frequencies of a simply supported power law FG Euler–Bernoulli beam based on the classical analysis ($b = 1\,\mu$m, $L = 10\,\mu$m, $E_m = 210$ GPa, $E_c = 390$ GPa, $k = 1$)

	$L/h = 20$			$L/h = 50$			$L/h = 100$		
	Mode 1	Mode 2	Mode 3	Mode 1	Mode 2	Mode 3	Mode 1	Mode 2	Mode 3
Present (GDQM)	6.9885	27.8602	62.3374	6.9951	27.9653	62.8655	6.9961	27.9804	62.9418
Ebrahimi and Salari [69]	6.9889	–	–	6.9951	–	–	6.9960	–	–
Attia [20]	7.0964	28.2988	63.3502	7.1026	28.3963	63.8392	7.1034	28.4103	63.91
Eltaher et al. [70]	7.0904	28.091	63.6216	7.0852	28.0048	63.1454	7.0833	27.9902	63.0799

Table 3 Comparison of dimensionless linear classical frequencies of a simply supported sigmoid FG Euler–Bernoulli beam based on the classical analysis ($b = 1\,\mu$m, $h = 0.1\,\mu$m, $L = 10\,\mu$m, $E_m = 70$ GPa, $E_c = 380$ GPa, $k = 1$)

	Mode 1	Mode 2	Mode 3
Present GDQM	14.6181	58.4645	131.5162
Hamed et al. [71]	15.7215	58.9333	136.4318

Table 4 Comparison of fundamental linear frequency (MHZ) of a simply supported homogeneous beam based on the classical and fully nonclassical analyses ($E = 90$ GPa, $\rho = 2700$, $\nu = 0.23$, $l = 6.58\,\mu$m, $\lambda^s = 3.4939$ N/m, $\mu^s = -5.4251$ N/m, $\tau^s = 0.5689$ N/m, $L = 20$ h and $b = 2$ h)

Beam theory	Solution method	Classical elasticity theory				Couple stress-surface energy theory			
		$h/l = 1$	$h/l = 6$	$h/l = 11$	$h/l = 16$	$h/l = 1$	$h/l = 6$	$h/l = 11$	$h/l = 16$
EBBT	Present GDQM	6.7222	1.1204	0.6111	0.4201	15.3425	1.1842	0.6217	0.4236
	Gao [22]	6.7222	1.1204	0.6111	0.4201	15.3416	1.1841	0.6217	0.4236
TBT	Present GDQM	6.6995	1.1166	0.6090	0.4187	15.2474	1.1801	0.6196	0.4222
	Gao [22]	6.6995	1.1166	0.6090	0.4187	15.2465	1.1801	0.6196	0.4222

Table 5 Material properties of the constituents of an FGM micro-/nanobeam

Property	Aluminum [100]	Silicon [100]
Bulk properties		
Young's modulus (GPa)	$E^B_{Al} = 90$	$E^B_{Si} = 210$
Poisson's ratio	$\nu_{Al} = 0.23$	$\nu_{Si} = 0.24$
Bulk density (kg/m^3)	$\rho^B_{Al} = 2700$	$\rho^B_{Si} = 2331$
Material length scale parameter (μm)	$l_{Al} = 6.58$	–
Surface properties		
Surface density (kg/m^2 $\times$ 10^7)	$\rho^s_{Al} = 5.46$	$\rho^s_{Si} = 3.1688$
Surface residual stress (N/m)	$\tau^s_{Al} = 0.5689$	$\tau^s_{Si} = 0.6056$
Surface Lamé modulus (N/m)	$\mu^s_{Al} = -5.4251$	$\mu^s_{Si} = -2.7779$
Surface Lamé modulus (N/m)	$\lambda^s_{Al} = 3.4939$	$\lambda^s_{Si} = -4.4939$
Surface elastic modulus (N/m)	$E^s_{Al} = -7.3563$	$E^s_{Si} = -10.0497$

frequency of simply supported homogeneous nanobeams is obtained using EBBT and TBT and compared with Gao [22] as reported in Table 4 showing an excellent agreement.

4.2 Comparison of Pseudo-arclength and Runge–Kutta methods

In contrast to the linear frequency response of a dynamic system, the nonlinear frequency response depends on the nonlinear amplitude. The solution of the nonlinear system of ordinary differential equations (Eq. (41)) provides the frequency–response relationship of the nonclassical nonlinear free vibration of FG nanobeams. As mentioned in the previous Sect. 3.3, two methodologies have been employed for solving Eq. (41): Runge–Kutta method and pseudo-arclength continuation technique.

Based on the developed integrated model that incorporates the simultaneous effects of couple stress and surface energy (CSSER) and considering the material properties provided in Table 5, the first vibration mode

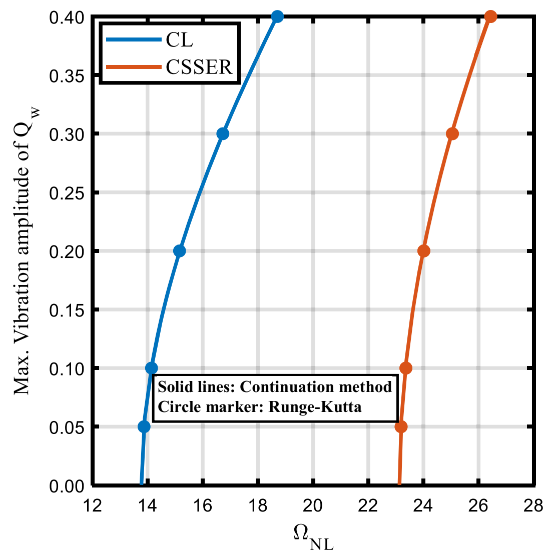

Fig. 2 Comparison of solution methodologies for the frequency response of a simply supported FG nanobeam ($k = 1$, $l_m = 6.58\,\mu$m, $l_c/l_m = 1.5$, $b = h$, $L/h = 15$, $h/l_m = 2$)

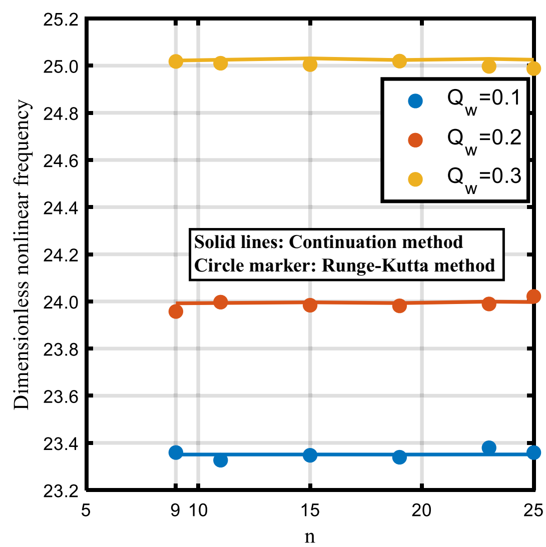

Fig. 3 Convergence of GDQM with pseudo-arclength and Runge–Kutta methods for the nonlinear frequency of simply supported FG nanobeam based on the CSSER model ($k = 1$, $l_m = 6.58\,\mu$m, $l_c/l_m = 1.5$, $b = h$, $L/h = 15$, $h/l_m = 2$)

for a simply supported FG Timoshenko beam using Runge–Kutta and pseudo-arclength continuation methods is illustrated in Fig. 2. These results are obtained at $k = 1$, $l_c/l_m = 1.5$, $b = h$, $L/h = 15$, and $h/l_m = 2$. It is seen that both methods agree with each other for CSSER as well as the classical analyses. Despite this agreement, the computational time of the Runge–Kutta method is larger than that of the pseudo-arclength continuation method. The pseudo-arclength continuation method is only suitable for steady-state responses, as in this study, while the Runge–Kutta method is sufficient for both transient and steady-state responses.

It should be mentioned that although Eq. (41) governs the response as a function of time (or equivalently, nonlinear frequency), the coefficients of this equation depend on the computed static responses and the linear vibration modes. Thus, the effect of the number of grid points n along the beam length on the convergence of the nonlinear frequency is investigated. Figure 3 shows the dimensionless nonlinear frequency of the simply supported FG Timoshenko nanobeam at different numbers of grid points and nonlinear amplitudes based on the CSSER model. It is clear that the present solution methodologies are well converged for $n \geq 11$. From

Table 1 and Fig. 3, it can be concluded that using a considerably smaller number of grid points, GDQM can obtain very accurate numerical results for linear and nonlinear frequencies.

5 Parametric study

In this Section, the proposed model is utilized to figure out the effect of the various bulk and surface material parameters on the frequency response of FG Timoshenko micro-/nanobeams, such as the bulk modulus of elasticity ratio ($E_r = E_c^B/E_m^B$), dimensionless material length scale parameter (h/l_m, l_c/l_m), surface elastic modulus $\left(E_c^s, E_m^s\right)$, surface residual stress $\left(\tau_c^s, \tau_m^s\right)$, gradient index ($k$), and beam thickness ($h$). Also, the influence of the nonclassical boundary conditions (NCBCs) is investigated for simply supported beams. Moreover, to explore the effect of the homogenization technique of the functionally graded materials, the results are obtained using power law and sigmoid function schemes.

For this purpose, consider an FGM beam made of aluminum (Al) and silicon (Si) with the bulk and surface material properties tabulated in Table 5 [22,25,49,62,72,73]. However, there are no available data of the material length scale parameter for silicon (l_{Si}) or functionally graded materials $l(z)$ in the open literature. In addition, the relation between the bulk and surface material properties and dimensions needs an experimental work, which is also not reported in the open literature. Several studies have been performed to investigate the effect of the material length scale parameter on the response of micro /nanostructures by supposing a range of h/l for homogeneous or FGM beams and plates [9,74,75]. To overcome the problem of the unknown value of l_{Si}, it can be assumed as a ratio of l_{AL} [5,76–78]. In all of the preceding numerical results, the length and width are selected as the ratios of, respectively, $L/h = 15$ and $b/h = 1$, unless other values of the material or geometrical parameters are mentioned.

5.1 Effect of the bulk modulus of the elasticity ratio

In this study, the effect of the bulk modulus of the elasticity ratio, i.e., $E_r = E_c^B/E_m^B$, on the linear and nonlinear vibration responses of FG beams based on the classical analysis is investigated, considering both sigmoid function and power law for the material gradation. The following results are obtained by keeping the elastic modulus of the metallic bulk material E_m^B constant at 90 GPa, while that of the ceramic bulk material E_c^B is controlled by the variation of E_r. The dimensions are as follows: $h = 2l_m = 13.16\,\mu$m, $b = h$, and $L = 15\,h$. It is seen from Fig. 4 that increasing the ratio E_r increases the bulk equivalent stiffness D_{xx}, defined in Eq. (17.1), of both SIG-FG and PL-FG beams. On the other hand, as the gradient index increases, D_{xx} is slightly decreased for SIG-FG and increased for PL-FG beam. However, employing SIG-FG or PL-FG

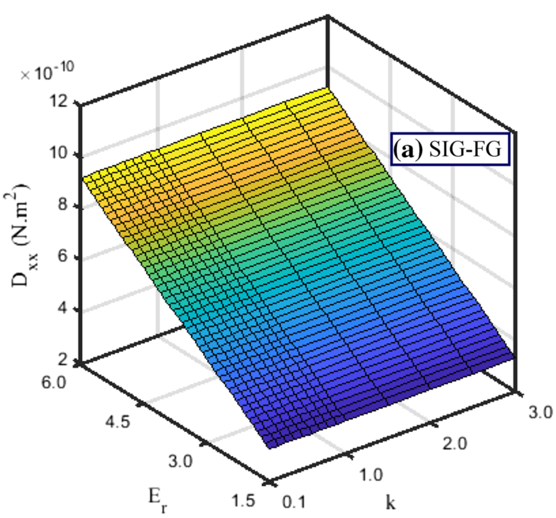

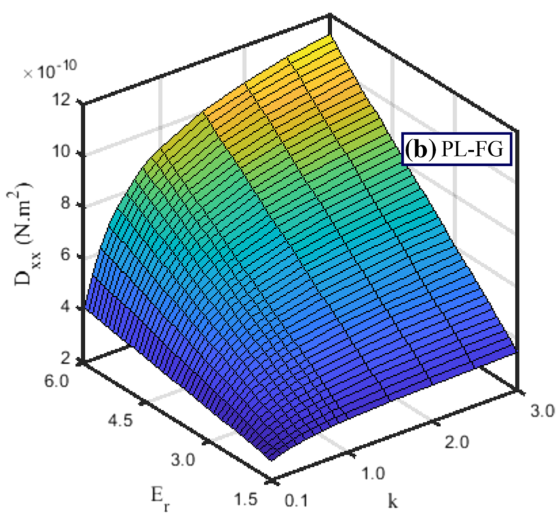

Fig. 4 Variation of the bulk equivalent stiffness D_{xx} of an FG microbeam with the bulk modulus of elasticity ratio and the gradient index, **a** SIG-FG and **b** PL-FG

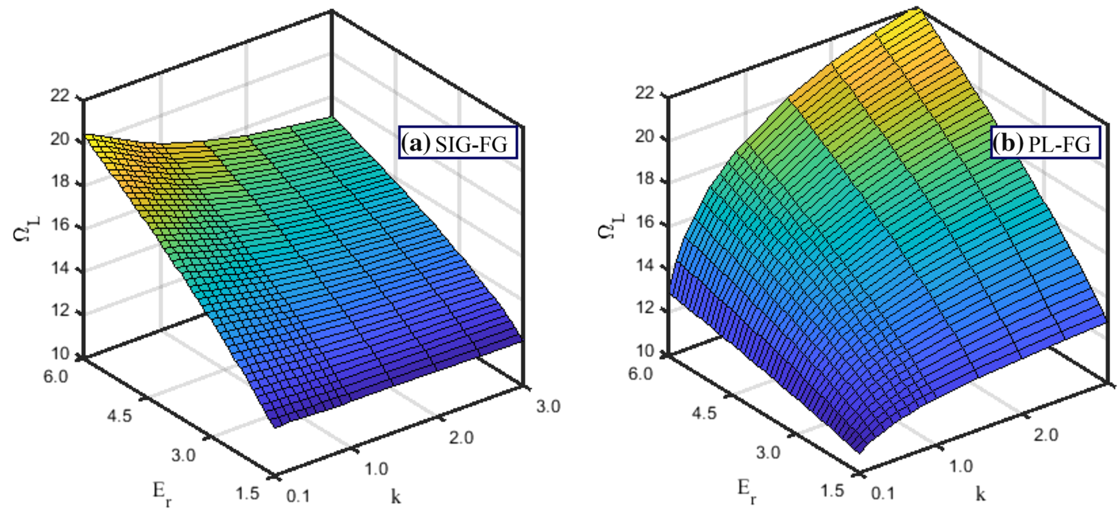

Fig. 5 Variation of the dimensionless fundamental linear frequency of a simply supported FG microbeam with E_r and k based on the classical analysis, **a** SIG-FG and **b** PL-FG

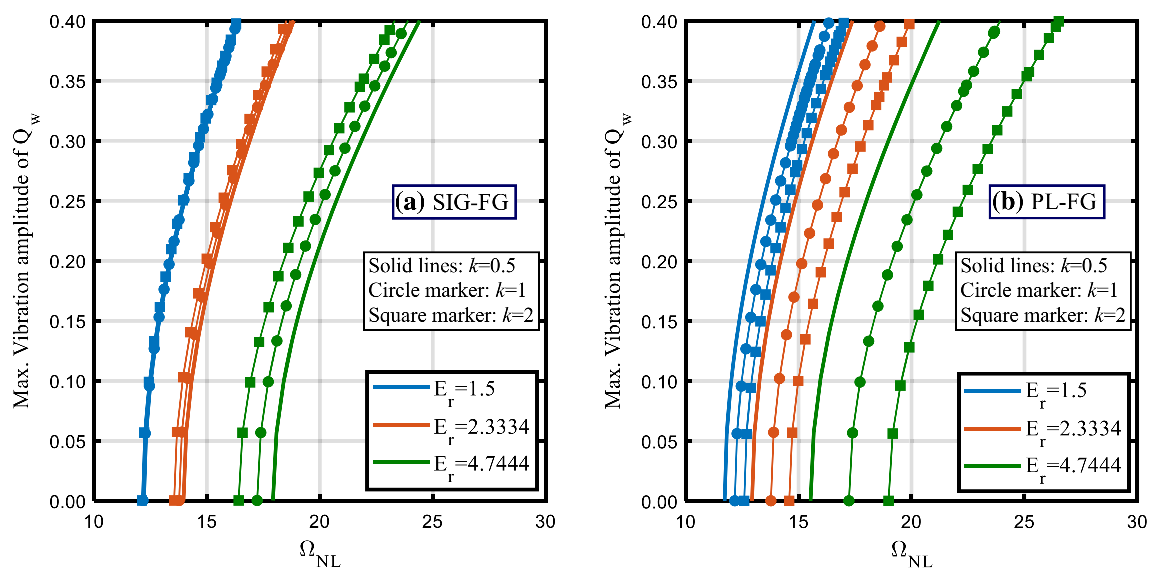

Fig. 6 Variation of the dimensionless fundamental nonlinear frequency versus the maximum nonlinear amplitude of a simply supported FG microbeam at different values of E_r and k based on the classical analysis, **a** SIG-FG and **b** PL-FG

homogenization technique leads to the same beam stiffness at $k = 1$, and consequently, they yield an identical vibration response.

Based on the results shown in Fig. 4, increasing the ratio E_r noticeably increases the dimensionless fundamental linear and nonlinear frequencies of the simply supported FG beam, as figured out in Figs. 5 and 6, respectively. Table 6 tabulates the dimensionless fundamental linear and nonlinear frequencies of the simply supported and clamped–clamped beams for different values of E_r and k. From these results, it is seen that the effects of E_r and k on the fundamental linear and nonlinear frequencies show a similar trend as the linear frequency is the starting value for estimating the nonlinear frequency. The fundamental frequencies of the simply supported and clamped–clamped beams are influenced by E_r and k in a similar way, except that the frequencies of the clamped–clamped beam are larger than those of the simply supported due to the additional stiffness induced by the clamped end. In addition, increasing the gradient index significantly decreases or increases the effect of the ratio E_r in the case of SIG-FG and PL-FG beams, respectively. For a simply supported beam at $Q_w = 0.2$, changing E_r from 1.5 to 4.744, i.e., E_c^B changes from 135 to 427 GPa (SiC), respectively, the fundamental nonlinear frequency of simply supported microbeam is increased by 47.6, 43.2,

Table 6 Dimensionless fundamental linear and nonlinear frequencies of simply supported and clamped–clamped SIG-FG and PL-FG microbeams based on the classical analysis ($h = 2l_\mathrm{m}$, $b = h$, $L/h = 15$)

E_r	k	Simply supported				Clamped–clamped			
		Ω_L	Ω_NL			Ω_L	Ω_NL		
			$Q_w = 0.1$	0.2	0.3		$Q_w = 0.1$	0.2	0.3
Sigmoid FG material distribution									
1.50	0.5	12.2222	12.5304	13.4004	14.7291	27.0636	27.1967	27.4790	28.0105
	1	12.1804	12.4899	13.3647	14.7080	26.9752	27.0781	27.4171	27.9111
	2	12.1331	12.4410	13.3207	14.675	26.8748	26.9784	27.3158	27.8147
2.333	0.5	13.9727	14.3217	15.3511	16.9029	30.9536	31.0615	31.4677	32.0601
	1	13.7782	14.1556	15.1707	16.7503	30.5413	30.6597	31.0489	31.6824
	2	13.5568	13.9233	14.9779	16.5523	30.0711	30.1979	30.6022	31.2050
4.744	0.5	17.9299	18.4100	19.7796	21.8335	39.7591	39.9432	40.4446	41.2259
	1	17.2297	17.7279	19.1364	21.2711	38.2686	38.4808	38.9552	39.8249
	2	16.4115	16.9443	18.4063	20.6199	36.5178	36.7089	37.2744	38.1371
Power law FG material distribution									
1.50	0.5	11.7307	12.0177	12.8519	14.1242	25.9695	26.075	26.3145	26.8832
	1	12.1804	12.4899	13.3647	14.7080	26.9752	27.0781	27.4171	27.9111
	2	12.5970	12.9290	13.8581	15.2739	27.9108	28.007	28.3544	28.9563
2.333	0.5	12.9431	13.2737	14.2038	15.6167	28.6641	28.7865	29.0932	29.6993
	1	13.7782	14.1556	15.1707	16.7503	30.5413	30.6597	31.0489	31.6824
	2	14.5882	14.9914	16.1156	17.8273	32.3608	32.4674	32.9261	33.6366
4.744	0.5	15.5332	15.9628	17.1574	18.9666	34.4578	34.6668	35.0684	35.7621
	1	17.2297	17.7279	19.1364	21.2711	38.2686	38.4808	38.9552	39.8249
	2	18.9837	19.5603	21.1560	23.5567	42.1870	42.4171	42.9649	43.9465

and 38.2% (SIG-FG) and 33.5, 43.2, and 52.7% (PL-FG) for k of 0.5, 1, and 2, respectively. The effect of the ratio E_r on the linear vibration response is found to be slightly lower than on the nonlinear response.

Moreover, as the vibration amplitude increases, the fundamental nonlinear frequency of the FG beams increases. In addition, incorporating the geometrical nonlinearity due to von Kármán's strain increases the frequencies as the beam becomes stiffer. However, the influence of the geometrical nonlinearity on the vibration response of a simply supported beam is higher than that of a clamped–clamped beam as its contribution depends on the structure degree of freedom, i.e., the degree of freedom of a simply supported end is higher than for the clamped–clamped end type.

5.2 Effect of the material length scale parameter

The microstructure length scale parameter introduced in MCST is an inherent material parameter, and thus, it may have different values for different materials. The length scale parameter for specific materials is determined experimentally [79,80] or using the atomistic simulations method [81]. Since the material length scale parameter is not experimentally determined for all different materials, some developed formulations of functionally graded microbeams were based on the assumption of constant material length scale parameter [9,74,75]. The present model treats the material length scale parameter as a variable according to the proposed gradation schemes. The material length scale parameter of the metallic constituent is held constant at $l_\mathrm{m} = 6.58\,\mu\mathrm{m}$, as provided in Table 5, and that of the ceramic constituent is taken as a ratio of l_m as $(l_\mathrm{c}/l_\mathrm{m})$ [5,76–78]. The results in this parametric study are obtained based on incorporating the effect of microstructure only (CS analysis).

Figure 7 demonstrates the variation of the dimensionless fundamental linear frequency of the simply supported FG microbeams versus the material length scale parameter ratio $(l_\mathrm{c}/l_\mathrm{m})$ and the gradient index (k). It is depicted that increasing the ratio $l_\mathrm{c}/l_\mathrm{m}$ increases the stiffness–hardening of the microbeam, and hence, the fundamental linear frequency increases. For the same ratio $l_\mathrm{c}/l_\mathrm{m}$, employing the SIG-FG law yields a higher linear frequency compared with PL-FG law when $k < 1$, whereas an opposite behavior is detected when $k > 1$. Such behavior can be explained in light of the fact that the in-plane shear stiffness coefficient (S_{xy}) is the only quantity that depends on $l(z)$, as shown in Eq. (17.1). It is noticed from Fig. 8 that for a certain value of the ratio $l_\mathrm{c}/l_\mathrm{m}$, S_{xy} of SIG-FG is higher than that of PL-FG microbeam for k less than unity and vice versa for k larger than unity. In Fig. 9, the dimensionless fundamental linear frequency of the simply supported FG microbeam is presented as a function of the ratio $l_\mathrm{c}/l_\mathrm{m}$ and h/l_m at $k = 0.5$. For a better illustration, selected numerical

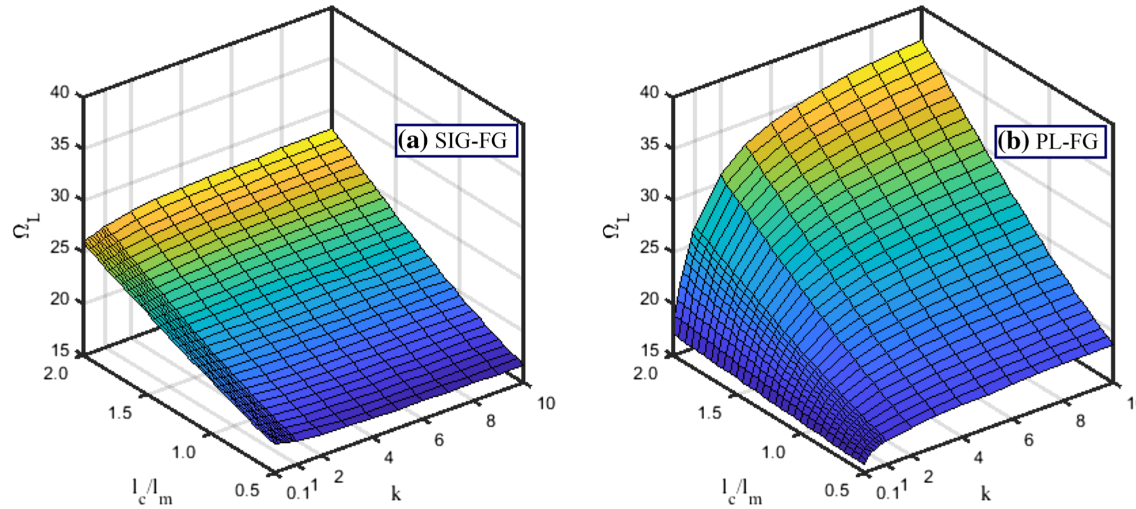

Fig. 7 Variation of the dimensionless fundamental linear frequency of a simply supported FG microbeam with l_c/l_m and k based on the CS analysis ($l_m = 6.58\,\mu$m, $b = h$, $L/h = 15$, $h/l_m = 2$), **a** SIG-FG and **b** PL-FG

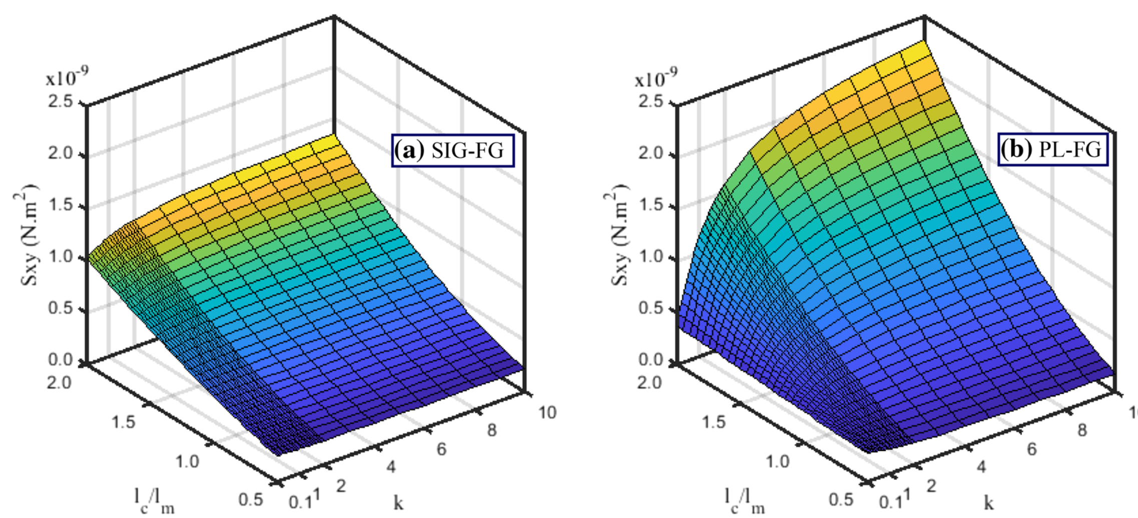

Fig. 8 Variation of the in-plane shear stiffness coefficient S_{xy} of an FG microbeam with l_c/l_m and k ($l_m = 6.58\,\mu$m, $b = h$, $L/h = 15$, $h/l_m = 2$), **a** SIG-FG and **b** PL-FG

values of the dimensionless fundamental linear frequency of the simply supported and clamped–clamped FG nanobeams are tabulated in Tables 7 and 8 for different values of l_c/l_m, h/l_m, and k, considering SIG-FG and PL-FG laws. The results show that the dimensionless linear frequencies predicted by the classical microbeam model are independent of the material length scale parameters, and their values are lower than those computed based on the couple stress analysis. This is attributed to that incorporating the effect of couple stress makes a microbeam stiffer and consequently leads to an increase in the vibration frequencies. Generally, this effect can be ignored when h/l_m becomes large as demonstrated in Fig. 9. Additionally, it is noticed that as the material length scale parameter of the ceramic component becomes larger compared to that of the metallic component (l_c/l_m), the vibration frequency of the FG microbeam becomes larger significantly.

In addition, based on the results in Figs. 8 and 9 and Tables 7 and 8, it is observed that the values of the fundamental linear frequencies based on a position-independent material length scale parameter, i.e., $l_c = l_m$, are distinctly different from those predicted based on a position-dependent material length scale parameter, i.e., $l_c \neq l_m$, especially with the growth of l_c/l_m or l_m/h. With the increase in h/l_m, the effect of the material length scale parameter ratio becomes inconspicuous. Also, the effect of the material length scale parameter ratio on increasing the fundamental linear frequency of both SIG-FG and PL-FG microbeams becomes more notable as the gradient index increases. For the simply supported FG microbeam with $h/l_m = 2$, increasing

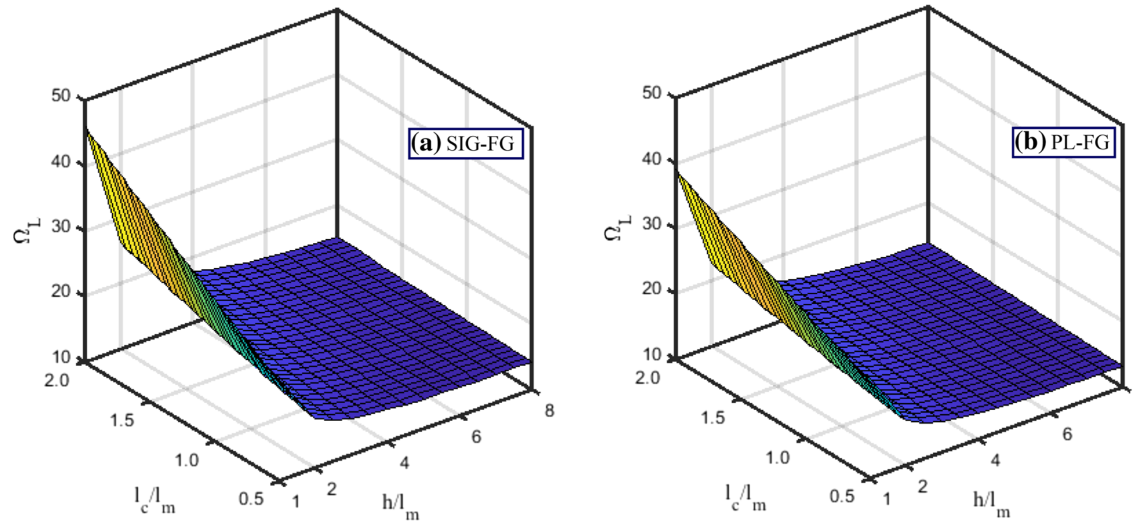

Fig. 9 Variation of the dimensionless fundamental linear frequency of a simply supported FG microbeam with l_c/l_m and h/l_m based on the CS analysis ($l_m = 6.58\,\mu$m, $b = h$, $L/h = 15$, $k = 0.5$), **a** SIG-FG and **b** PL-FG

Table 7 Dimensionless fundamental linear frequency of simply supported SIG-FG and PL-FG microbeams based on CS analysis ($l_m = 6.58\,\mu$m, $b = h$, $L/h = 15$)

$\frac{l_c}{l_m}$	$h/l_m = 1$				$h/l_m = 2$				$h/l_m = 5$			
	Gradient index k											
	0.5	1	2	10	0.5	1	2	10	0.5	1	2	10
Sigmoid FG material distribution												
1/2	25.4712	25.1341	24.7274	24.1036	17.5841	17.3453	17.0651	16.6886	14.6116	14.4093	14.1775	13.9041
1.0	31.9120	31.8263	31.7296	31.6197	20.0732	19.9379	19.7849	19.6129	15.1181	14.9384	14.7343	14.5043
3/2	38.9180	39.3682	39.9156	40.8471	23.0221	23.1320	23.2764	23.5849	15.7807	15.6627	15.5347	15.4283
2.0	46.1709	47.2752	48.5871	50.7138	26.2693	26.7034	27.2321	28.1468	16.5803	16.5563	16.5428	16.6212
CL	20.2534	20.2933	20.3542	20.5358	15.7832	15.6676	15.5423	15.4403	14.2781	14.0978	13.8939	13.6710
Power law FG material distribution												
1/2	25.1978	25.1341	24.8815	24.6137	16.8848	17.3453	17.7422	18.7219	13.6517	14.4093	15.1377	16.6964
1.0	29.4069	31.8263	34.1779	37.7377	18.5321	19.9379	21.3040	23.6124	13.9908	14.9384	15.8583	17.6637
3/2	34.1081	39.3682	44.6042	52.2470	20.4887	23.1320	25.7823	29.8923	14.4235	15.6627	16.8961	19.1366
2.0	39.0976	47.2752	55.3695	66.9458	22.6716	26.7034	30.7605	36.8208	14.9414	16.5563	18.1960	21.0074
CL	21.8114	20.2933	18.8265	17.3603	15.6489	15.6676	15.7566	16.5579	13.4133	14.0978	14.7815	16.3262

Table 8 Dimensionless fundamental linear frequency of clamped–clamped SIG-FG and PL-FG microbeams based on CS analysis ($l_m = 6.58\,\mu$m, $b = h$, $L/h = 15$)

$\frac{l_c}{l_m}$	$h/l_m = 1$				$h/l_m = 2$				$h/l_m = 5$			
	Gradient index k											
	0.5	1	2	10	0.5	1	2	10	0.5	1	2	10
Sigmoid FG material distribution												
1/2	56.0205	55.3198	54.4711	53.1571	38.9371	38.4309	37.8350	37.0286	32.3726	31.9431	31.4498	30.8658
1.0	69.5689	69.4113	69.2331	69.0291	44.3813	44.1050	43.7921	43.4392	33.4964	33.1176	32.6865	32.1995
3/2	83.8204	84.7378	85.8477	87.7140	50.7694	51.0249	51.3567	52.0429	34.9630	34.7213	34.4593	34.2466
2.0	97.9681	100.0840	102.5752	106.5512	57.7203	58.6619	59.8043	61.7614	36.7282	36.6940	36.6849	36.8802
CL	44.7737	44.8789	45.0320	45.4492	34.9686	34.7321	34.4761	34.2732	31.6308	31.2501	30.8187	30.3467
Power law FG material distribution												
1/2	55.2798	55.3198	54.9105	54.4210	37.3658	38.4309	39.3478	41.5093	30.2378	31.9431	33.5812	37.0177
1.0	64.0949	69.4113	74.5777	82.3139	40.9638	44.1050	47.1570	52.2420	30.9900	33.1176	35.1820	39.1667
3/2	73.7057	84.7378	95.6496	111.4061	45.2076	51.0249	56.8478	65.7953	31.9479	34.7213	37.4800	42.4254
2.0	83.6071	100.0840	116.1171	138.6084	49.9025	58.6619	67.4353	80.4094	33.0922	36.6940	40.3477	46.5438
CL	48.0574	44.8789	41.7343	38.4935	34.6516	34.7321	34.9564	36.7092	29.7082	31.2501	32.7879	36.1922

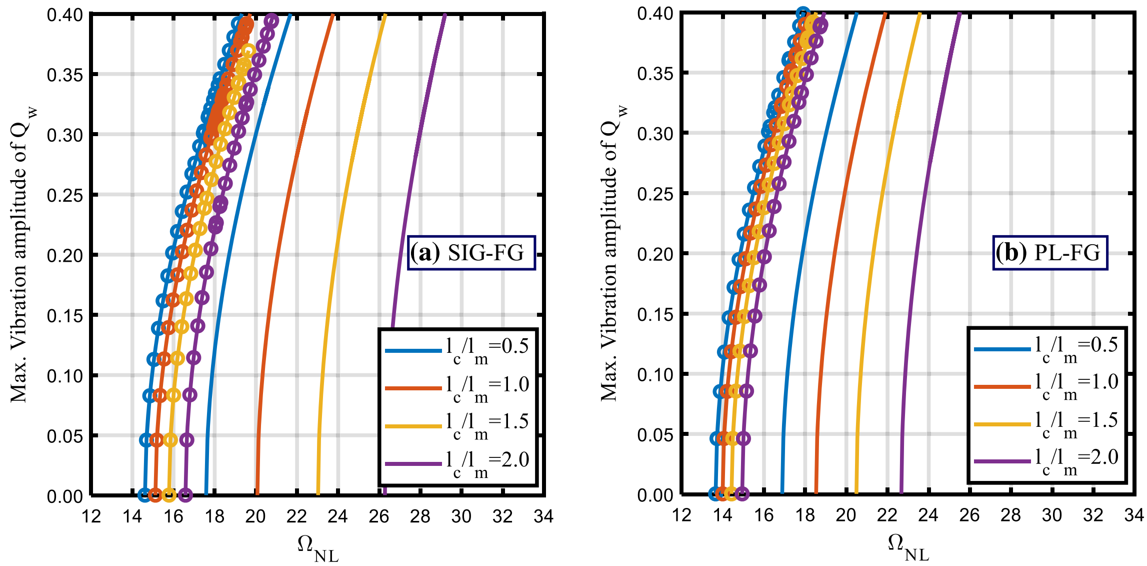

Fig. 10 Variation of the dimensionless fundamental nonlinear frequency versus the maximum nonlinear amplitude of a simply supported FG microbeam at different values of l_c/l_m and h/l_m based on the CS analysis ($l_m = 6.58\,\mu$m, $b = h$, $L/h = 15$, $k = 0.5$), **a** SIG-FG and **b** PL-FG. Solid lines: at $h/l_m = 2$; circle markers: at $h/l_m = 5$

Table 9 Combined effects of l_m/l_c and h/l_m on the dimensionless fundamental nonlinear frequency of simply supported SIG-FG and PL-FG microbeams based on CS analysis ($l_m = 6.58\,\mu$m, $b = h$, $L/h = 15$)

Q_w	$\frac{l_c}{l_m}$	$h/l_m = 1$				$h/l_m = 2$				$h/l_m = 5$			
		Gradient index k											
		0.5	1	2	10	0.5	1	2	10	0.5	1	2	10
Sigmoid FG material distribution													
0.1	1/2	25.6847	25.3546	24.9529	24.3170	17.8673	17.6401	17.3579	16.9928	14.9541	14.7581	14.5389	14.2573
	1.0	32.0979	31.9935	31.8872	31.8052	20.3247	20.1906	20.0393	19.8658	15.4557	15.2740	15.0735	14.8471
	3/2	39.0261	39.5575	40.0774	40.9666	23.2481	23.3577	23.5080	23.8117	16.0885	15.9908	15.8715	15.7530
	2.0	46.2714	47.3732	48.7372	50.7870	26.4696	26.9129	27.4451	28.3693	16.8759	16.8569	16.8543	16.9253
	CL	20.5054	20.5416	20.5868	20.7782	16.0941	15.9923	15.8567	15.7593	14.6332	14.4561	14.2642	14.0370
0.2	1/2	26.2328	25.9325	25.5417	24.9199	18.6893	18.4827	18.2006	17.8789	15.9361	15.7499	15.5248	15.2964
	1.0	32.5497	32.4625	32.3417	32.2863	21.0673	20.9315	20.7777	20.6149	16.3942	16.2301	16.0448	15.8345
	3/2	39.4800	39.9539	40.4210	41.4053	23.8580	23.9825	24.1288	24.4152	17.0235	16.9012	16.8017	16.6758
	2.0	46.6088	47.7007	48.9851	51.1175	27.0263	27.4702	27.9414	28.8581	17.7608	17.7282	17.7247	17.8089
	CL	21.2224	21.2683	21.3352	21.5142	17.0130	16.9078	16.7800	16.7099	15.6319	15.4710	15.2802	15.0878
0.3	1/2	27.2439	26.8781	26.5004	25.9280	20.0161	19.7833	19.5408	19.2229	17.4358	17.2673	17.0844	16.8329
	1.0	33.3818	33.1921	33.1202	33.0594	22.2140	22.1092	21.9575	21.8267	17.8463	17.7037	17.5421	17.3462
	3/2	40.0719	40.4973	41.0253	41.9328	24.9505	24.9966	25.1682	25.4989	18.4315	18.3403	18.2200	18.1444
	2.0	47.2811	48.2769	49.4401	51.6084	27.9449	28.3611	28.8680	29.7388	19.1057	19.1079	19.0826	19.1640
	CL	22.3840	22.4247	22.4698	22.6707	18.4430	18.3508	18.2348	18.1351	17.1549	17.0073	16.8460	16.6480
Power law FG material distribution													
0.1	1/2	25.3950	25.3546	25.1374	24.9154	17.1312	17.6401	18.0613	19.0993	13.9531	14.7581	15.5208	17.1232
	1.0	29.5603	31.9935	34.3453	37.9057	18.7723	20.1906	21.5668	23.9119	14.2947	15.2740	16.2259	18.0750
	3/2	34.2267	39.5575	44.7688	52.3156	20.6925	23.3577	26.0353	30.1218	14.7094	15.9908	17.2433	19.5071
	2.0	39.2112	47.3732	55.5088	66.9282	22.8715	26.9129	30.9556	37.0318	15.2304	16.8569	18.5124	21.3482
	CL	21.9875	20.5416	19.1405	17.7731	15.9133	15.9923	16.1206	16.9908	13.7340	14.4561	15.1745	16.7621
0.2	1/2	25.8590	25.9325	25.8258	25.7399	17.8630	18.4827	19.0337	20.1998	14.8367	15.7499	16.6248	18.3257
	1.0	30.0110	32.4625	34.8631	38.4732	19.4289	20.9315	22.3804	24.8112	15.1685	16.2301	17.2768	19.2171
	3/2	34.6127	39.9539	45.0569	52.9138	21.3096	23.9825	26.6802	30.8561	15.5690	16.9012	18.2241	20.5945
	2.0	39.5562	47.7007	55.6216	67.2833	23.4023	27.4702	31.5546	37.6293	16.0330	17.7282	19.4547	22.3299
	CL	22.5668	21.2683	20.0322	18.9264	16.6946	16.9078	17.1907	18.2076	14.6303	15.4710	16.2965	17.9948
0.3	1/2	26.6628	26.8781	26.9205	27.1325	19.0296	19.7833	20.4983	21.8735	16.2117	17.2673	18.2772	20.1939
	1.0	30.6557	33.1921	35.6690	39.4603	20.5043	22.1092	23.6521	26.2043	16.5029	17.7037	18.9002	20.9833
	3/2	35.2319	40.4973	45.7937	53.4221	22.3094	24.9966	27.7504	31.9725	16.8712	18.3403	19.7677	22.2636
	2.0	40.1145	48.2769	56.3905	68.0568	24.3347	28.3611	32.4663	38.4916	17.3273	19.1079	20.9087	23.8761
	CL	23.4937	22.4247	21.4404	20.7400	17.9310	18.3508	18.8037	20.0769	16.0187	17.0073	17.9894	19.8704

Table 10 Combined effects of l_m/l_c and h/l_m on the dimensionless fundamental nonlinear frequency of clamped–clamped SIG-FG and PL-FG microbeams based on CS analysis ($l_m = 6.58\,\mu m$, $b = h$, $L/h = 15$)

Q_w	$\frac{l_c}{l_m}$	$h/l_m = 1$				$h/l_m = 2$				$h/l_m = 5$			
		Gradient index k											
		0.5	1	2	10	0.5	1	2	10	0.5	1	2	10
Sigmoid FG material distribution													
0.1	1/2	56.1318	55.4722	54.4243	53.2278	39.0852	38.5029	37.9265	37.1340	32.5015	32.0973	31.5506	30.9879
	1.0	69.9449	69.4016	69.2129	69.1096	44.4406	44.2813	43.9362	43.4949	33.6082	33.2397	32.8184	32.2597
	3/2	83.4346	84.5114	86.2404	87.5991	50.9004	51.1732	51.4631	52.1387	35.1250	34.8477	34.6071	34.3437
	2.0	98.0608	100.2685	102.9438	106.6455	57.7926	58.7170	59.7213	61.8256	36.8726	36.7871	36.8034	37.0209
	CL	44.9190	44.9227	45.2226	45.6211	35.0585	34.8743	34.5971	34.4114	31.7955	31.3987	30.9664	30.5025
0.2	1/2	56.1564	55.5897	54.6612	53.3943	39.3397	38.8177	38.2865	37.4764	32.8298	32.4661	31.9502	31.3977
	1.0	69.6648	69.6579	69.3172	69.3628	44.7986	44.4850	44.2409	43.9324	34.0001	33.6162	33.1275	32.6769
	3/2	84.2303	84.6345	86.3403	87.9538	51.0266	51.2495	51.6237	52.3896	35.3958	35.1316	34.9288	34.7103
	2.0	98.3963	100.5292	102.7992	106.7250	58.0578	59.0873	60.0221	61.9719	37.1132	37.1319	37.1507	37.2968
	CL	45.1444	45.2348	45.4261	45.7413	35.4453	35.2190	34.9793	34.7641	32.1404	31.7353	31.2933	30.7922
0.3	1/2	56.7146	55.8709	55.2513	53.8603	39.8510	39.3156	38.7457	38.0284	33.4748	33.0167	32.6028	32.0245
	1.0	69.9685	69.9151	69.9638	69.6583	45.1368	44.9278	44.5772	44.2274	34.5089	34.1773	33.7955	33.2938
	3/2	84.5056	85.4650	86.1174	88.1129	51.4524	51.7400	52.1092	52.6845	35.9648	35.7288	35.5096	35.3094
	2.0	98.3678	100.5876	103.1445	106.6069	58.3316	59.1097	60.2965	62.4401	37.6751	37.6777	37.6063	37.8683
	CL	45.4790	45.6916	45.7997	46.1226	35.9547	35.7583	35.4574	35.2952	32.7310	32.3629	31.9593	31.5545
Power law FG material distribution													
0.1	1/2	55.1481	55.4722	55.0410	54.5088	37.5013	38.5029	39.5259	41.7150	30.3601	32.0973	33.7094	37.1752
	1.0	64.3301	69.4016	74.7415	82.6563	40.9998	44.2813	47.2811	52.3756	31.0722	33.2397	35.3480	39.3342
	3/2	73.7354	84.5114	95.8253	111.3791	45.3217	51.1732	56.9717	65.8834	32.0388	34.8477	37.5959	42.5740
	2.0	83.3120	100.2685	115.8341	138.9459	49.9111	58.7170	67.5889	80.6374	33.2227	36.7871	40.4416	46.6443
	CL	48.0578	44.9227	41.8271	38.6160	34.7123	34.8743	35.0492	36.8645	29.8333	31.3987	32.8974	36.3317
0.2	1/2	55.5554	55.5897	55.2090	54.8579	37.7365	38.8177	39.8612	42.0934	30.6486	32.4661	34.1178	37.6381
	1.0	64.1769	69.6579	74.6252	82.5946	41.2955	44.4850	47.5763	52.7331	31.4225	33.6162	35.7042	39.7764
	3/2	73.8740	84.6345	95.5707	111.2685	45.4909	51.2495	57.1973	65.9776	32.3686	35.1316	38.0063	43.0235
	2.0	84.0862	100.5292	116.1699	138.4749	50.2016	59.0873	67.6864	80.8686	33.5227	37.1319	40.7872	46.9709
	CL	48.3154	45.2348	42.2417	39.1117	35.0421	35.2190	35.5081	37.2916	30.1821	31.7353	33.2971	36.7139
0.3	1/2	55.7669	55.8709	55.7296	55.3663	38.1656	39.3156	40.3796	42.7086	31.2107	33.0167	34.7860	38.3627
	1.0	64.5728	69.9151	75.1013	83.1697	41.7323	44.9278	48.0346	53.1556	31.8875	34.1773	36.3257	40.4887
	3/2	74.1538	85.4650	95.8211	111.9751	45.9003	51.7400	57.6725	66.5387	32.8640	35.7288	38.6136	43.5397
	2.0	84.1065	100.5876	117.1220	138.2415	50.5682	59.1097	67.9540	80.9957	34.0228	37.6777	41.3641	47.5672
	CL	48.6424	45.6916	42.7470	39.7931	35.4923	35.7583	36.1331	38.0173	30.7181	32.3629	34.0484	37.5595

l_c/l_m from 0.5 to 2 shows an increase in the dimensionless linear frequency by about 49.4, 54, 68.7% (SIG-FG) and 34.3, 54, 96.7% (PL-FG) for a gradient index k of 0.5, 1, 10, respectively. In addition, as the dimensionless material length scale parameter h/l_m increases from 1 to 5 and at $k = 0.5$, the dimensionless linear frequency is decreased by about 42.6, 52.6, 64.1% (SIG-FG) and 45.8, 52.4, 61.8% (PL-FG) for l_c/l_m of 0.5, 1, and 2, respectively. In addition, it is noticeable that the effect of the ratio l_c/l_m on the fundamental linear frequency of the simply supported and clamped–clamped FG microbeams is similar to a negligible difference.

Considering the nonlinear vibration response, the dimensionless fundamental nonlinear frequency Ω_{NL} versus the maximum nonlinear vibration amplitude Q_w is plotted in Fig. 10 for various values of the ratio l_c/l_m, two different values of h/l_m of 2 and 5, and $k = 0.5$. Tables 9 and 10 include the values of Ω_{NL} at different Q_w, l_c/l_m, h/l_m, and k. It is noticed that the combined effects of geometric nonlinearity and couple stress result in more hardening for the simply supported FG microbeam when compared with the clamped–clamped one. Also, the influences of l_c/l_m and h/l_m on Ω_{NL} of the clamped–clamped FG microbeam are slightly larger than those for a simply supported microbeam, and these influences are much more significant when the gradient index increases. As mentioned before, this is attributed to that the microbeam becomes stiffer as l_c becomes larger than l_m or l_m is smaller than h. One can notice that the dimensionless nonlinear frequency is considerably increased by increasing l_c/l_m and significantly reduced by decreasing h/l_m. For $Q_w = 0.2$ and $h/l_m = 2$, as l_c/l_m increases from 0.5 to 2, Ω_{NL} increases by about 44.6, 48.6, and 61.4% (SS SIG-FG), 31, 48.6, and 86.3% (SS PL-FG), 47.6, 52.2, and 65.4% (CC SIG-FG), and 33, 52.2, and 92.1% (CC PL-FG) for k of 0.5, 1, and 10, respectively. Also, Ω_{NL} of the clamped–clamped FG microbeam changes slightly by varying Q_w. In addition, comparing the results in Tables 7 , 8, 9, and 10, it is depicted that the effects of l_c/l_m and h/l_m on the nonlinear frequency response are less significant than those on the linear response.

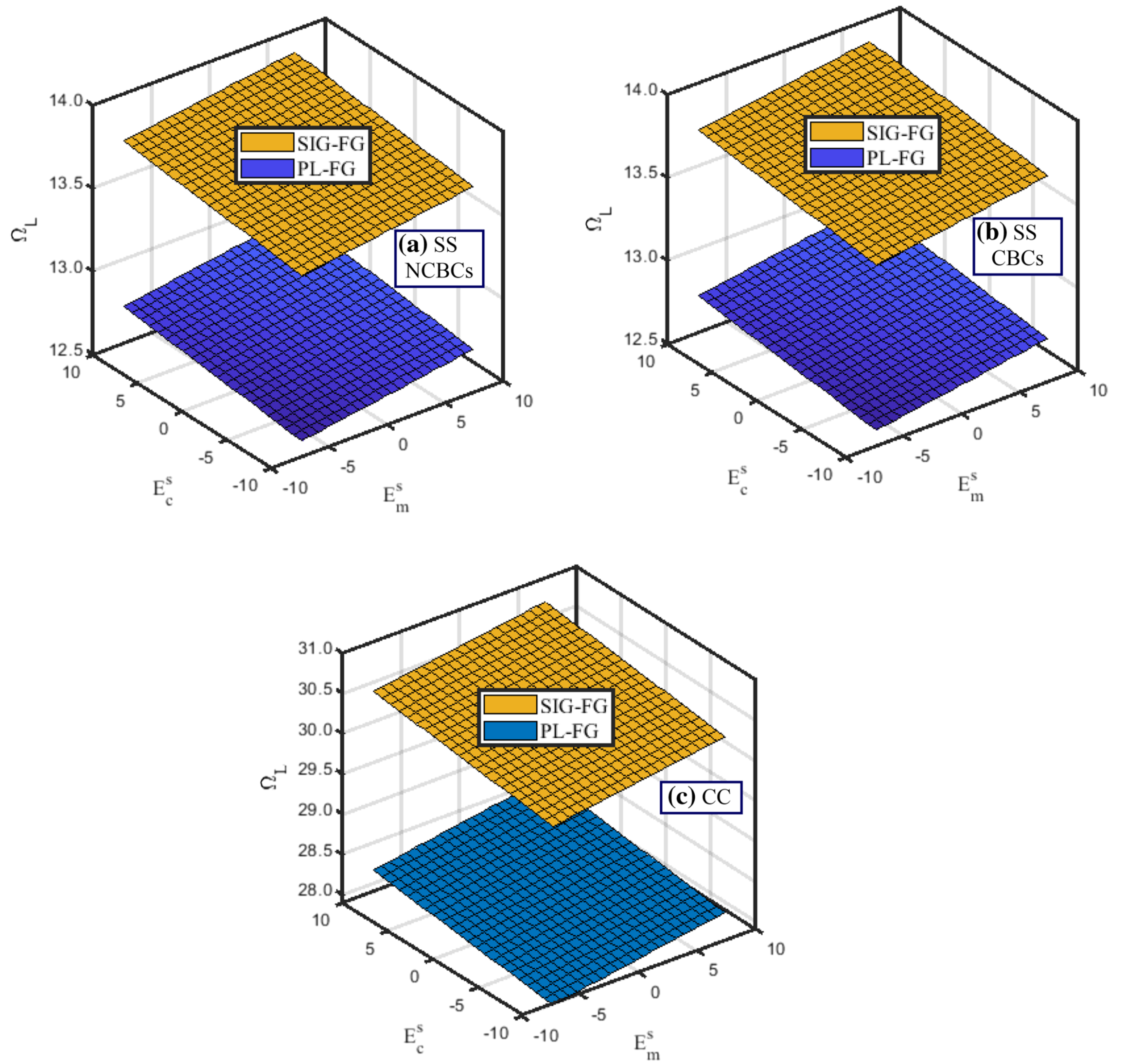

Fig. 11 Variation of the dimensionless fundamental linear frequency of SIG-FG and PL-FG nanobeams with $E_{\mathrm{m}}^{\mathrm{s}}$ and $E_{\mathrm{c}}^{\mathrm{s}}$ ($k = 0.5$), **a** simply supported with NCBCs, **b** simply supported with CBCs, and **c** clamped–clamped

However, the obtained results reveal that the dimensionless linear and nonlinear frequencies are very sensitive to the variations in the ratio $l_{\mathrm{c}}/l_{\mathrm{m}}$, especially at $h/l_{\mathrm{m}} = 1$. In addition, the effect of h/l_{m} is considerably influenced by $l_{\mathrm{c}}/l_{\mathrm{m}}$. At $k = 0.5$ and $Q_w = 0.2$, increasing h/l_{m} of a simply supported microbeam from 1 to 5 reduces Ω_{NL} by about 39.9, 49.6, and 61.9% (SS SIG-FG), 42.6, 49.5, and 59.5% (SS PL-FG), 41.5, 51.2, and 62.3% (CC SIG-FG), and 44.8, 51, and 60.1% (CC PL-FG) for $l_{\mathrm{c}}/l_{\mathrm{m}}$ of 0.5, 1, and 2, respectively. It can be generally concluded that the material length scale parameter should be considered as spatial-dependent function ($l(z)$) in either a linear or nonlinear analysis of small-scale FG beams, as proposed in the present study.

5.3 Effect of surface energy

The effect of surface parameters, surface elasticity modulus ($E^{\mathrm{s}}(z)$), and surface residual stress ($\tau^{\mathrm{s}}(z)$), on the linear and nonlinear vibration responses is explored for FG simply supported and clamped–clamped nanobeams with $h = 20\,\mathrm{nm}$, $b = h$, and $L/h = 15$. Both sigmoid and power law gradation schemes are investigated using the bulk and surface material properties provided in Table 5, in the absence of a microstructure effect.

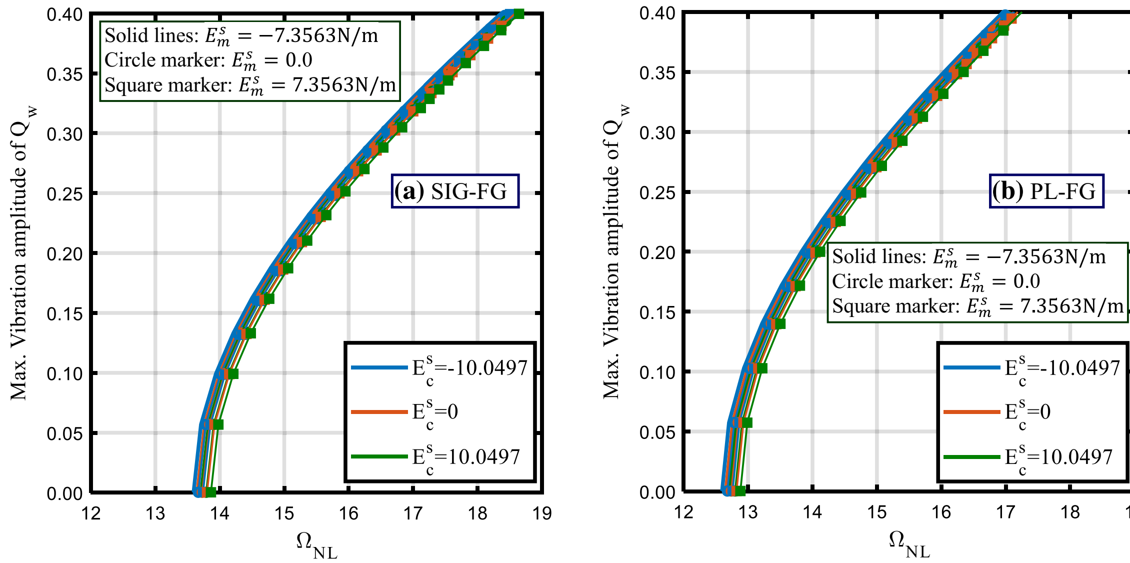

Fig. 12 Variation of the dimensionless fundamental nonlinear frequency versus the maximum nonlinear amplitude of a simply supported FG nanobeam at different values of $E_{\mathrm{m}}^{\mathrm{s}}$ and $E_{\mathrm{c}}^{\mathrm{s}}$ ($k = 0.5$), **a** SIG-FG and **b** PL-FG

5.3.1 Effect of surface elastic modulus

The influence of the surface elasticity modulus of the metallic and ceramic constituents, $E_{\mathrm{m}}^{\mathrm{s}}$ and $E_{\mathrm{c}}^{\mathrm{s}}$, respectively, on the dimensionless linear frequency of FG nanobeams at $k = 0.5$ is demonstrated in Fig. 11 when the surface residual stress is ignored. Figure 12 shows the variation of the dimensionless nonlinear frequency of the simply supported FG nanobeams versus the nonlinear amplitude at different values of $E_{\mathrm{m}}^{\mathrm{s}}$ and $E_{\mathrm{c}}^{\mathrm{s}}$. The dimensionless fundamental linear and nonlinear frequencies in this study are tabulated in Tables 11 and 12. From these results, it can be easily found that the positive surface modulus of elasticity of the metallic ($E_{\mathrm{m}}^{\mathrm{s}}$) or the ceramic material ($E_{\mathrm{c}}^{\mathrm{s}}$) increases the first-mode linear frequencies. The main trend is that the fundamental linear and nonlinear frequencies are slightly increased by increasing $E_{\mathrm{m}}^{\mathrm{s}}$ and $E_{\mathrm{c}}^{\mathrm{s}}$ simultaneously or individually. The effects of $E_{\mathrm{m}}^{\mathrm{s}}$ and $E_{\mathrm{c}}^{\mathrm{s}}$, when the bulk material follows SIG-FG, are lower than those when following PL-FG. Also, the surface elasticity moduli have a slight impact on the fundamental nonlinear frequency compared with the linear frequency. Generally, it can be concluded that the positive surface elasticity moduli add stiffness to the system and thus result in larger linear and nonlinear frequencies, whereas an opposite effect is noticed for negative values.

5.3.2 Effect of surface residual stress

The dimensionless fundamental linear frequency of FG nanobeams versus the surface residual stresses ($\tau_{\mathrm{m}}^{\mathrm{s}}$ and $\tau_{\mathrm{c}}^{\mathrm{s}}$) is shown in Fig. 13 at k= 0.5 and $E_{\mathrm{c}}^{\mathrm{s}} = E_{\mathrm{m}}^{\mathrm{s}}$= 0, while the variation of the dimensionless fundamental nonlinear frequency versus the amplitude of nonlinearity is depicted in Fig. 14 for various values of $\tau_{\mathrm{m}}^{\mathrm{s}}$ and $\tau_{\mathrm{c}}^{\mathrm{s}}$. The values of the dimensionless linear and nonlinear frequencies of the simply supported and clamped–clamped FG nanobeams are provided in Tables 13 and 14 for different values of $\tau_{\mathrm{m}}^{\mathrm{s}}$, $\tau_{\mathrm{c}}^{\mathrm{s}}$, k, and nonlinear amplitude. In view of these results, it can be seen that the positive values of the surface residual stresses increase the fundamental linear and nonlinear frequencies, and negative values tend to decrease the frequencies. Like the effect of surface elasticity moduli, positive surface residual stresses stiffen the FG nanobeam and in turn lead to higher linear and nonlinear frequencies. The presence of the surface residual stresses dependent terms in simply supported boundary conditions (NCBCs), i.e., $\mathcal{P}_1^*/2$ and $C_1^*/2$ in Eq. (28.1) acts as self-excitation loading and causes deformation of the FG nanobeam at no external load. As a consequence, the impact of the surface residual stress on the linear and nonlinear frequencies of simply supported FG nanobeams is larger than that of clamped–clamped ends. Comparing between Figs. 11 and 13 as well as Figs. 12 and 14 shows that the effect of the surface residual stress on the frequency response is considerably more pronounced than that of the surface elasticity modulus.

Table 11 Combined effects of $E_{\mathrm{m}}^{\mathrm{s}}$, $E_{\mathrm{c}}^{\mathrm{s}}$, and k on the dimensionless fundamental linear frequency of FG nanobeams ($h = 20\,\mathrm{nm}$, $b = h$, $L/h = 15$, $E_{m0}^{\mathrm{s}} = -7.3563\,\mathrm{N/m}$, $E_{c0}^{\mathrm{s}} = -10.0497\,\mathrm{N/m}$)

$\frac{E_{\mathrm{c}}^{\mathrm{s}}}{E_{c0}^{\mathrm{s}}}$	$\frac{E_{\mathrm{m}}^{\mathrm{s}}}{E_{m0}^{\mathrm{s}}}$	Simply supported			Clamped–clamped		
		Gradient index k					
		0.5	1	2	0.5	1	2
Sigmoid FG material distribution							
1	1	13.5927	13.4078	13.1954	30.1248	29.7333	29.2824
	0	13.6668	13.4855	13.2761	30.2817	29.8980	29.4540
	−1	13.7401	13.5622	13.3558	30.4367	30.0606	29.6233
0	1	13.6542	13.4693	13.2584	30.2549	29.8638	29.4164
	0	13.7283	13.5470	13.3391	30.4119	30.0285	29.5878
	−1	13.8017	13.6238	13.4188	30.5670	30.1912	29.7570
−1	1	13.7149	13.5301	13.3208	30.3835	29.9927	29.5489
	0	13.7892	13.6079	13.4015	30.5405	30.1575	29.7203
	−1	13.8626	13.6848	13.4812	30.6957	30.3202	29.8894
Power law FG material distribution							
1	1	12.5969	13.4078	14.2124	27.9097	29.7333	31.5396
	0	12.6793	13.4855	14.2823	28.0841	29.8980	31.6883
	−1	12.7607	13.5622	14.3515	28.2560	30.0606	31.8353
0	1	12.6574	13.4693	14.2783	28.0375	29.8638	31.6796
	0	12.7399	13.5470	14.3482	28.2121	30.0285	31.8282
	−1	12.8214	13.6238	14.4175	28.3841	30.1912	31.9752
−1	1	12.7171	13.5301	14.3436	28.1637	29.9927	31.8182
	0	12.7997	13.6079	14.4135	28.3383	30.1575	31.9668
	−1	12.8813	13.6848	14.4828	28.5105	30.3202	32.1137

Table 12 Combined effects of $E_{\mathrm{m}}^{\mathrm{s}}$, $E_{\mathrm{c}}^{\mathrm{s}}$, and k on the dimensionless fundamental nonlinear frequency of FG nanobeams ($h = 20\,\mathrm{nm}$, $b = h$, $L/h = 15$, $E_{m0}^{\mathrm{s}} = -7.3563\,\mathrm{N/m}$, $E_{c0}^{\mathrm{s}} = -10.0497\,\mathrm{N/m}$)

$\frac{E_{\mathrm{c}}^{\mathrm{s}}}{E_{c0}^{\mathrm{s}}}$	$\frac{E_{\mathrm{m}}^{\mathrm{s}}}{E_{m0}^{\mathrm{s}}}$	Simply supported						Clamped–clamped					
		$k = 0.5$			$k = 2.0$			$k = 0.5$			$k = 2.0$		
		$Q_w = 0.1$	0.2	0.3	$Q_w = 0.1$	0.2	0.3	$Q_w = 0.1$	0.2	0.3	$Q_w = 0.1$	0.2	0.3
Sigmoid FG material distribution													
1	1	13.9437	14.9495	16.4684	13.5529	14.5881	16.1358	30.2612	30.6640	31.1988	29.3844	29.8084	30.4099
	0	14.0116	15.0204	16.5424	13.6277	14.6676	16.2175	30.3869	30.8206	31.4475	29.5478	29.9878	30.5947
	−1	14.0941	15.0859	16.6039	13.7150	14.7355	16.3183	30.5668	30.8731	31.5436	29.7554	30.1576	30.7185
0	1	14.0065	15.0063	16.5208	13.6261	14.6619	16.2217	30.4101	30.7134	31.3623	29.5375	29.9319	30.5370
	0	14.0857	15.0711	16.5973	13.6946	14.7275	16.2926	30.4875	30.9264	31.5056	29.6979	30.1137	30.7226
	−1	14.1584	15.1600	16.6903	13.7817	14.8062	16.3801	30.6612	31.0880	31.6625	29.8601	30.2558	30.8863
−1	1	14.0672	15.0852	16.5807	13.6857	14.7176	16.2911	30.5039	30.9001	31.4495	29.6864	30.0878	30.6779
	0	14.1415	15.1476	16.6752	13.7597	14.8011	16.3674	30.6647	31.0362	31.6787	29.8845	30.1948	30.8920
	−1	14.2107	15.2126	16.7384	13.8309	14.8697	16.4480	30.8145	31.1503	31.7435	30.0276	30.3813	30.9927
Power law FG material distribution													
1	1	12.9138	13.8302	15.2223	14.6148	15.7220	17.4020	28.0558	28.3686	28.8752	31.6706	32.0816	32.7553
	0	13.0080	13.9156	15.2981	14.6770	15.7892	17.4575	28.2047	28.5120	29.0641	31.8417	32.2512	32.8861
	−1	13.0791	13.9935	15.3826	14.7432	15.8690	17.5333	28.3828	28.7199	29.2439	31.9748	32.4217	33.0657
0	1	12.9717	13.8889	15.2819	14.6756	15.7915	17.4584	28.1634	28.4720	29.0132	31.7870	32.2018	32.9379
	0	13.0690	13.9723	15.3611	14.7313	15.8433	17.5549	28.3601	28.6437	29.2145	31.9347	32.3444	33.0629
	−1	13.1472	14.0562	15.4560	14.8080	15.9269	17.6167	28.4673	28.8665	29.3600	32.1588	32.5002	33.2058
−1	1	13.0305	13.9539	15.3496	14.7394	15.8591	17.5412	28.2761	28.5829	29.1416	31.9891	32.3615	33.0338
	0	13.1102	14.0288	15.4274	14.8173	15.9223	17.6005	28.4063	28.7957	29.3075	32.0932	32.5156	33.2407
	−1	13.2127	14.1156	15.5039	14.8712	15.9889	17.6834	28.6069	28.9722	29.5041	32.2536	32.6894	33.3397

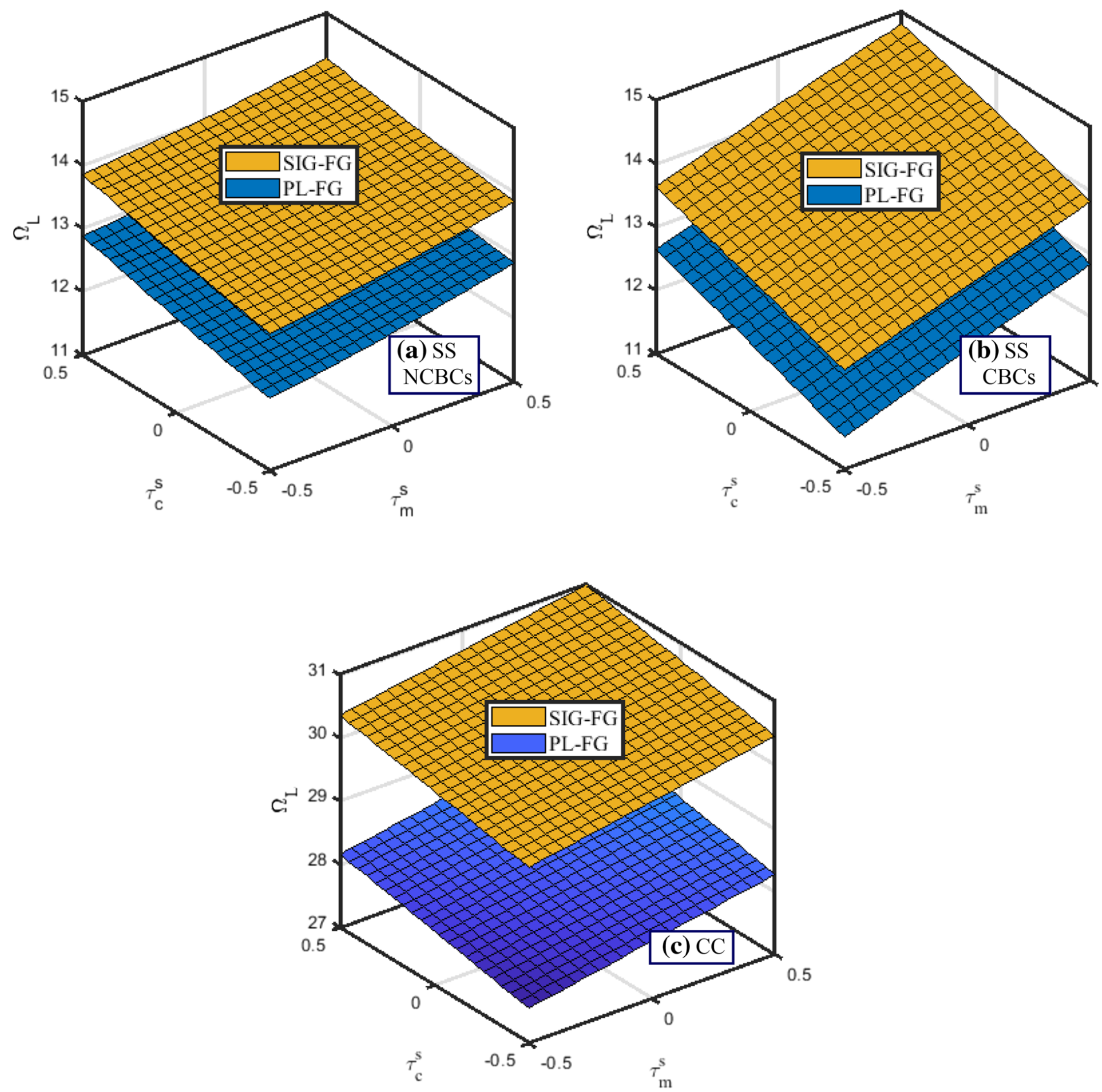

Fig. 13 Variation of the dimensionless fundamental linear frequency for SIG-FG and PL-FG nanobeams with τ_m^s and τ_c^s ($k = 0.5$), **a** simply supported with NCBCs, **b** simply supported with CBCs, and **c** clamped–clamped

5.4 Effect of the nonclassical boundary conditions

One of the contributions in the developed model and proposed solution procedure is applying the nonclassical (nonideal) boundary conditions (NCBCs) for simply supported FG nanobeams, represented by Eq. (28.1). In NCBCs besides, the nonlinearity in the boundaries' equations, there is a part of surface energy effect which contributes as an internal excited loading in the case of simply supported FG nanobeams. The effect of NCBCs on the dimensionless linear frequency of simply supported FG nanobeams is presented in Figs. 11a, b and 13a, b based on SE analysis. Also, a comparison between values of the dimensionless linear and nonlinear frequencies employing NCBCs and CBCs is presented in Tables 15 and 16, considering both surface energy (SE) and integrated couple stress-surface energy (CSSER) models. From these results, it can be extracted that for both SIG-FG and PL-FG nanobeams using NCBCs results in linear and nonlinear frequencies lower than those using CBCs for positive τ^s, whereas negative τ^s leads to an opposite effect. Varying E^s from a negative to a positive value has a significant effect on the contribution of NCBCs for negative τ^s, and this effect becomes very small to be negligible for positive τ^s. Also, the impact of NCBCs on the vibration response increases as the gradient index increases. Moreover, it can be concluded that NCBCs

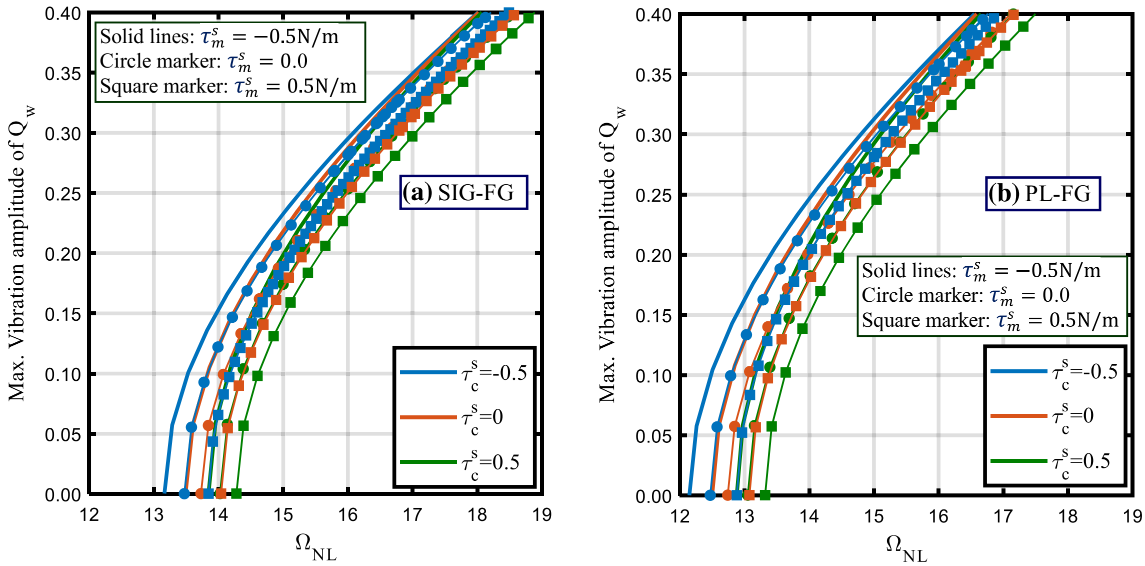

Fig. 14 Variation of the dimensionless fundamental nonlinear frequency versus the maximum nonlinear amplitude of a simply supported FG nanobeam at different values of $\tau_{\mathrm{m}}^{\mathrm{s}}$ and $\tau_{\mathrm{c}}^{\mathrm{s}}$ ($k = 0.5$), **a** SIG-FG and **b** PL-FG

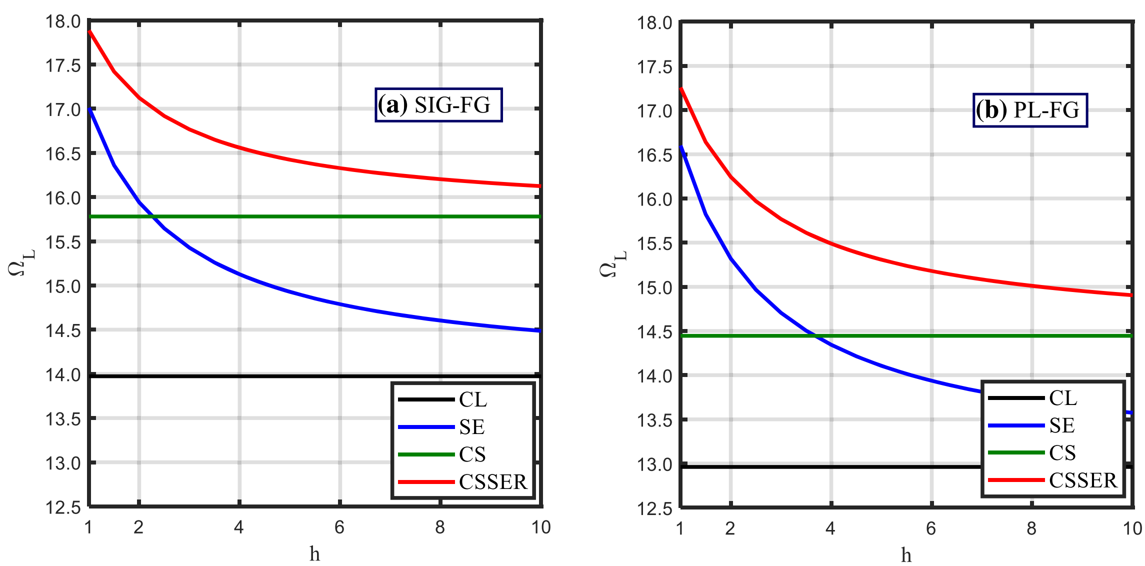

Fig. 15 Variation of the dimensionless fundamental linear frequency with the thickness of a simply supported FG nanobeam using different analyses ($k = 0.5$, $l_{\mathrm{m}} = 0.2\,\mathrm{h}$, $l_{\mathrm{c}} = 1.5 l_{\mathrm{m}}$, $L/h = 15$), **a** SIG-FG and **b** PL-FG

should not be neglected in the formulation of linear and nonlinear vibration problems of simply supported FG nanobeams.

5.5 Effect of nanobeam thickness

The variation of the dimensionless fundamental linear and nonlinear frequencies for the simply supported nanobeam at different thicknesses is considered in Figs. 15 and 16, respectively, based on the various analyses of SIG-FG and PL-FG distributions. The material parameters are those provided in Table 5 with $k = 0.5$, $l_{\mathrm{m}} = 0.2\,\mathrm{h}$, $l_{\mathrm{c}} = 1.5 l_{\mathrm{m}}$, and $L = 15\,\mathrm{h}$. Some values of the dimensionless fundamental linear and nonlinear frequencies, respectively, are reported in Tables 15 and 16 at different thicknesses of the simply supported FG nanobeam. It is noticeable that the dimensionless linear and nonlinear frequencies obtained by the classical elasticity (CL) and couple stress (CS) models are unaffected by varying the nanobeam thickness.

Table 13 Combined effects of $\tau_{\mathrm{m}}^{\mathrm{s}}$, $\tau_{\mathrm{c}}^{\mathrm{s}}$, and k on the dimensionless fundamental linear frequency of FG nanobeams ($h = 20\,\mathrm{nm}$, $b = h$, $L/h = 15$, $\tau_{m0}^{\mathrm{s}} = 0.5689\,\mathrm{N/m}$, $\tau_{c0}^{\mathrm{s}} = 0.6056\,\mathrm{N/m}$)

$\frac{\tau_{\mathrm{c}}^{\mathrm{s}}}{\tau_{c0}^{\mathrm{s}}}$	$\frac{\tau_{\mathrm{m}}^{\mathrm{s}}}{\tau_{m0}^{\mathrm{s}}}$	Simply supported			Clamped–clamped		
		Gradient index k					
		0.5	1	2	0.5	1	2
Sigmoid FG material distribution							
1	1	14.3692	14.1996	14.0059	31.1214	30.7501	30.3231
	0	14.0892	13.9121	13.7054	30.7505	30.4030	30.0000
	− 1	13.9070	13.7453	13.5362	30.3744	30.0514	29.6728
0	1	14.0868	13.9209	13.7238	30.7874	30.3804	29.9160
	0	13.7283	13.5470	13.3391	30.4119	30.0285	29.5878
	− 1	13.4636	13.2910	13.0847	30.0310	29.6719	29.2555
− 1	1	13.8694	13.7080	13.4986	30.4493	30.0057	29.5026
	0	13.4226	13.2358	13.0167	30.0690	29.6487	29.1691
	− 1	13.0612	12.8737	12.6595	29.6831	29.2869	28.8313
Power law FG material distribution							
1	1	13.4148	14.1996	14.9803	28.9578	30.7501	32.5296
	0	13.1192	13.9121	14.7007	28.5683	30.4030	32.2211
	− 1	12.9485	13.7453	14.5227	28.1726	30.0514	31.9092
0	1	13.1266	13.9209	14.7039	28.6071	30.3804	32.1410
	0	12.7399	13.5470	14.3482	28.2121	30.0285	31.8282
	− 1	12.4746	13.2910	14.0913	27.8107	29.6719	31.5120
− 1	1	12.9099	13.7080	14.4860	28.2514	30.0057	31.7471
	0	12.4185	13.2358	14.0447	27.8507	29.6487	31.4299
	− 1	12.0388	12.8737	13.6956	27.4433	29.2869	31.1090

Table 14 Combined effects of $\tau_{\mathrm{m}}^{\mathrm{s}}$, $\tau_{\mathrm{c}}^{\mathrm{s}}$, and k on the dimensionless fundamental nonlinear frequency of FG nanobeams ($h = 20\,\mathrm{nm}$, $b = h$, $L/h = 15$, $\tau_{m0}^{\mathrm{s}} = 0.5689\,\mathrm{N/m}$, $\tau_{c0}^{\mathrm{s}} = 0.6056\,\mathrm{N/m}$)

$\frac{\tau_{\mathrm{c}}^{\mathrm{s}}}{\tau_{c0}^{\mathrm{s}}}$	$\frac{\tau_{\mathrm{m}}^{\mathrm{s}}}{\tau_{m0}^{\mathrm{s}}}$	Simply supported						Clamped–clamped					
		$k = 0.5$			$k = 2.0$			$k = 0.5$			$k = 2.0$		
		$Q_w = 0.1$	0.2	0.3	$Q_w = 0.1$	0.2	0.3	$Q_w = 0.1$	0.2	0.3	$Q_w = 0.1$	0.2	0.3
Sigmoid FG material distribution													
1	1	14.7087	15.6760	17.1873	14.3473	15.3187	16.7944	31.2459	31.5674	32.1718	30.4330	30.7803	31.4114
	0	14.4255	15.4299	16.9806	14.0539	15.0161	16.4708	30.9152	31.2783	31.8005	30.1350	30.5195	31.1475
	− 1	14.1912	15.0230	16.3352	13.8709	14.9056	16.5977	30.4919	30.9041	31.4810	29.8087	30.1994	30.7876
0	1	14.4097	15.3528	16.8013	14.0869	15.1305	16.7856	30.9441	31.2859	31.8520	30.0749	30.4233	31.0162
	0	14.0857	15.0711	16.5973	13.6946	14.7275	16.2926	30.4875	30.9264	31.5056	29.6979	30.1137	30.7226
	− 1	13.8240	14.8614	16.4866	13.4178	14.3650	15.8097	30.1380	30.5165	31.1568	29.3632	29.7770	30.3925
− 1	1	14.1673	15.0693	16.5105	13.8409	14.9364	16.6868	30.5517	30.8966	31.5276	29.6573	29.9925	30.6209
	0	13.7922	14.8711	16.5143	13.3916	14.4941	16.1644	30.2131	30.5813	31.1775	29.3071	29.6951	30.2948
	− 1	13.4327	14.4487	16.0172	13.0369	14.1503	15.8076	29.7857	30.1647	30.7783	28.9600	29.3399	30.0062
Power law FG material distribution													
1	1	13.7322	14.6095	15.9670	15.3565	16.4184	18.0261	29.0436	29.3739	29.9295	32.6201	33.0554	33.7234
	0	13.4203	14.2529	15.5487	15.0818	16.1919	17.9194	28.6764	28.9888	29.5331	32.3830	32.7922	33.4253
	− 1	13.2423	14.1456	15.6514	14.8894	16.0297	17.8213	28.2893	28.6353	29.1942	32.0507	32.4290	33.1525
0	1	13.4373	14.3828	15.8595	15.0651	16.0971	17.6817	28.7133	29.0671	29.6119	32.2718	32.7198	33.3374
	0	13.0690	13.9723	15.3611	14.7313	15.8433	17.5549	28.3601	28.6437	29.2145	31.9347	32.3444	33.0629
	− 1	12.7828	13.6020	14.8803	14.4927	15.6531	17.4513	27.9357	28.2631	28.8141	31.6728	32.0536	32.7517
− 1	1	13.2300	14.2488	15.8811	14.8802	16.1021	18.0211	28.3785	28.6919	29.2514	31.8898	32.2956	32.9795
	0	12.7368	13.6274	14.9731	14.4491	15.6422	17.4530	27.9944	28.3184	28.8522	31.5627	31.9869	32.7362
	− 1	12.3738	13.3008	14.7245	14.1081	15.2849	17.0492	27.5462	27.9453	28.4437	31.2611	31.6768	32.4073

Table 15 Effect of the thickness on the dimensionless fundamental linear frequency of a simply supported FG nanobeam using different analyses with NCBCs and CBCs at various values of k and $h/l_{\mathrm{m}}(l_{\mathrm{c}}/l_{\mathrm{m}} = 1.5, L/h = 15)$

k	h (nm)	Dimensionless length scale parameter $h/l_{\mathrm{m}} = 0.2$						Dimensionless length scale parameter $h/l_{\mathrm{m}} = 0.5$					
		CL	SE		CS	CSSER		CL	SE		CS	CSSER	
			CBCs	NCBCs		CBCs	NCBCs		CBCs	NCBCs		CBCs	NCBCs
Sigmoid FG material distribution													
0.5	5	13.9728	16.9387	14.9281	15.7807	18.275	16.4229	13.9728	16.9387	14.9281	23.0221	24.0777	22.6983
	10	13.9728	15.6255	14.486	15.7807	17.1567	16.1236	13.9728	15.6255	14.486	23.0221	23.5912	22.849
	30	13.9728	14.5708	14.1525	15.7807	16.274	15.9003	13.9728	14.5708	14.1525	23.0221	23.2222	22.9616
1	5	13.7783	16.8485	14.8301	15.6627	18.2391	16.3777	13.7783	16.8485	14.8301	23.132	24.2376	22.8558
	10	13.7783	15.4883	14.3377	15.6627	17.0824	16.0411	13.7783	15.4883	14.3377	23.132	23.7269	22.9839
	30	13.7783	14.397	13.9722	15.6627	16.1713	15.7936	13.7783	14.397	13.9722	23.132	23.3409	23.0802
2	5	13.5569	16.7382	14.7188	15.5347	18.1946	16.3272	13.5569	16.7382	14.7188	23.2764	24.427	23.0447
	10	13.5569	15.3284	14.1679	15.5347	16.9988	15.9499	13.5569	15.3284	14.1679	23.2764	23.8942	23.1515
	30	13.5569	14.1979	13.7661	15.5347	16.0589	15.6769	13.5569	14.1979	13.7661	23.2764	23.493	23.2325
Power law FG material distribution													
0.5	5	12.9615	16.1587	14.1056	14.4454	17.2276	15.3067	12.9615	16.1587	14.1056	20.524	21.9834	20.4997
	10	12.9615	14.7515	13.5744	14.4454	15.9881	14.9046	12.9615	14.7515	13.5744	20.524	21.314	20.5092
	30	12.9615	13.6122	13.1752	14.4454	15.0012	14.6051	12.9615	13.6122	13.1752	20.524	20.8027	20.5183
2	5	14.5883	17.5500	15.5429	16.8961	19.2889	17.4705	14.5883	17.5500	15.5429	25.7823	26.5773	25.2792
	10	14.5883	16.2302	15.0958	16.8961	18.2073	17.1996	14.5883	16.2302	15.0958	25.7823	26.208	25.5151
	30	14.5883	15.1798	14.7644	16.8961	17.3636	17.001	14.5883	15.1798	14.7644	25.7823	25.9312	25.6894

Table 16 Effect of the thickness on the dimensionless fundamental nonlinear frequency of a simply supported FG nanobeam using different analyses with NCBCs and CBCs at various values of k and Q_w $(h/l_{\mathrm{m}} = 0.2, l_{\mathrm{c}}/l_{\mathrm{m}} = 1.5, L/h = 15)$

Q_w	h(nm)	Gradient index $k = 05$						Gradient index $k = 2$					
		CL	SE		CS	CSSER		CL	SE		CS	CSSER	
			CBCs	NCBCs		CBCs	NCBCs		CBCs	NCBCs		CBCs	NCBCs
Sigmoid FG material distribution													
0.1	5	14.3290	17.1883	15.2078	16.1062	18.5162	16.6742	13.9351	16.9800	14.9919	15.8451	18.4404	16.5805
	10	14.3290	15.9203	14.8131	16.1062	17.4355	16.4211	13.9351	15.6297	14.4762	15.8451	17.2736	16.2350
	30	14.3312	14.9152	14.5025	16.0989	16.5755	16.2059	13.9248	14.5444	14.1083	15.8612	16.3585	15.9824
0.2	5	15.3524	17.9146	16.0595	17.0116	19.2156	17.4129	14.9745	17.7379	15.7404	16.7849	19.100	17.3055
	10	15.3524	16.7533	15.7328	17.0116	18.2079	17.2479	14.9745	16.4977	15.3796	16.7849	18.0616	17.0392
	30	15.3512	15.8462	15.4915	17.0140	17.4334	17.0917	14.9640	15.5120	15.1183	16.7959	17.2400	16.8959
0.3	5	16.8986	19.0387	17.3728	18.4419	20.2638	18.5726	16.5476	18.8912	16.9218	18.2052	20.2023	18.4214
	10	16.8986	18.0765	17.1703	18.4419	19.4028	18.5644	16.5476	17.8362	16.7451	18.2052	19.3058	18.3109
	30	16.9014	17.3306	16.9947	18.4349	18.7798	18.4814	16.5542	17.0195	16.6266	18.2113	18.6128	18.2889
Power law FG material distribution													
0.1	5	13.2860	16.3875	14.3516	14.7396	17.4476	15.5478	14.988	17.8442	15.8703	17.2311	19.5303	17.7563
	10	13.2869	14.9998	13.8592	14.7259	16.2254	15.1598	14.9829	16.5652	15.4651	17.2498	18.4989	17.5188
	30	13.2904	13.9163	13.4895	14.7371	15.2861	14.8966	14.9849	15.5531	15.1555	17.2484	17.6842	17.3282
0.2	5	14.2045	17.0367	15.0343	15.5909	18.0591	16.1744	16.1196	18.6610	16.8054	18.2340	20.3060	18.5584
	10	14.2199	15.7628	14.6479	15.5842	16.9519	15.9066	16.1178	17.5126	16.5091	18.2564	19.3511	18.3977
	30	14.2146	14.7819	14.3951	15.5774	16.0601	15.706	16.1287	16.6089	16.2325	18.2290	18.6296	18.3098
0.3	5	15.6211	18.0372	16.1204	16.8894	18.9761	17.2315	17.8190	19.9313	18.3032	19.7773	21.4974	19.8128
	10	15.6193	16.9467	15.8718	16.8832	18.0512	17.0649	17.8202	18.9958	18.1055	19.7776	20.7145	19.8013
	30	15.6127	16.1019	15.7697	16.8973	17.2741	16.9862	17.8209	18.2419	17.8657	19.7856	20.1119	19.8177

Also, it is obvious that for surface energy (SE) and integrated couple stress-surface energy (CSSER) models increasing the thickness increases the dimensionless linear and nonlinear frequencies, and their values approach those obtained by the classical elasticity model. Such behavior is due to that the surface layer area-to-the bulk volume ratio is reduced by increasing thickness, and thus, a reduction in surface energy effect is detected.

In addition, the inclusion of NCBCs decreases the contribution of surface energy to the linear and nonlinear responses, especially at large values of the nanobeam thickness, and this effect is decreased by increasing the gradient index or nanobeam thickness. Moreover, increasing the gradient index of SIG-FG and PL-FG nanobeams, respectively, reduces and increases the surface energy effect in both SE and

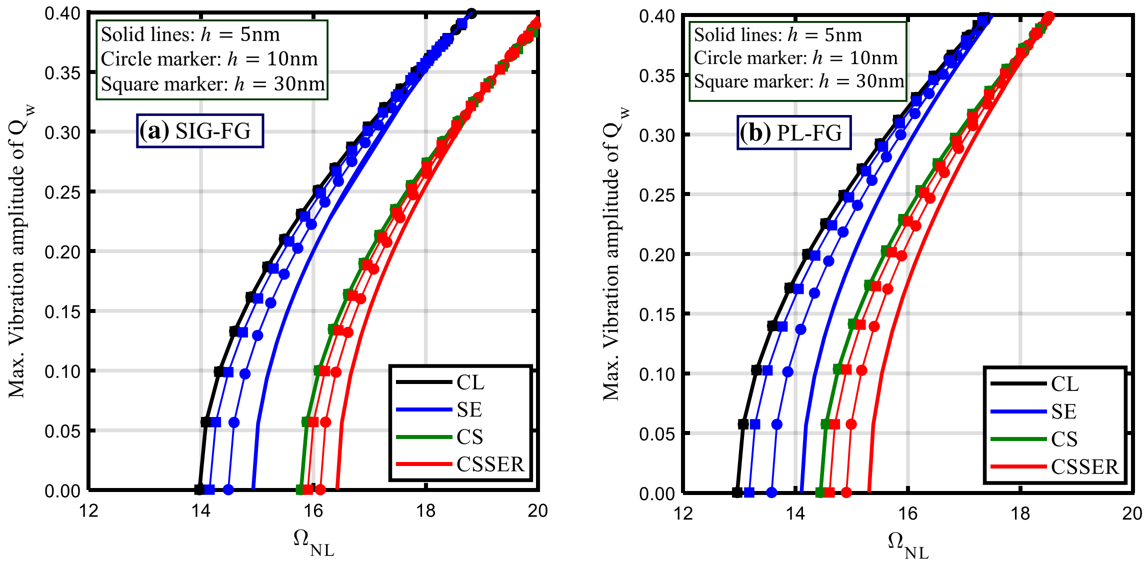

Fig. 16 Variation of the dimensionless fundamental nonlinear frequency versus the maximum nonlinear amplitude of a simply supported FG nanobeam using different analyses ($k = 0.5$, $l_m = 0.2h$, $l_c = 1.5l_m L/h = 15$), **a** SIG-FG and **b** PL-FG

CSSER models. This is observed for all nonlinear vibration amplitudes regardless of employing NCBCs or CBCs.

6 Conclusions

In this article, a continuum mechanics model is developed to study the nonlinear vibration response of FG Timoshenko nanobeams considering the nonlinear von Kármán strains. In order to account for the size-dependent effects, modified couple stress and Gurtin–Murdoch surface elasticity theories are employed. All the bulk and surface properties of the FG nanobeam material are assumed to vary across the thickness based on sigmoid and power law distribution functions. The nonlinear governing equations and corresponding nonideal boundary conditions are exactly derived according to Hamilton's principle, and then, GDQM was employed to discretize them in the spatial domain with an exact implementation of the nonideal boundary conditions. Runge–Kutta and pseudo-arclength continuation methods are used to obtain the nonlinear free vibration responses. By a comprehensive parametric study, the effects of bulk modulus of elasticity, surface energy, material length scale, and small-scale parameters are investigated for both sigmoid and power law FG micro-/nanobeams. The following main conclusions can be extracted from this study as below.

Consideration of classical boundary conditions (CBCs) tends to overestimate the fundamental natural frequencies Ω_L and Ω_{NL} for the simply supported FG nanobeams having positive surface residual stress, while for negative surface residual stress, the natural frequency is underestimated. This effect is increased by increasing or decreasing the gradient index of, respectively, SIG-FG or PL-FG nanobeams. Moreover, the natural frequencies increase with the increase in surface elasticity theory parameters, surface residual stresses, and surface elasticity moduli, due to the induced stiffness-hardening effect, especially for very thin beams. The influence of surface parameters becomes more significant by decreasing or increasing the gradient index of SIG-FG or PL-FG nanobeams, respectively.

The dimensionless material length scale parameter h/l_m and material length scale parameter ratio l_c/l_m have opposite effects; increasing l_c/l_m results in the stiffness-hardening effect, while increasing h/l_m limits the local-microstructure effect. Depending on h/l_m and the gradient index, l_c/l_m can display a dominant or ignored effect for both SIG-FG and PL-FG micro-/nanobeams. Also, spatial variation of the material length scale parameter should be considered in the analysis of FG beams. In addition, the combined effect of nonlinearity, couple stress, and positive surface parameters results in more stiffness-hardening for the FG nanobeam, especially with simply supported ends. For CSSER analysis, the local-microstructure effect becomes the dominant one at larger thicknesses whereas by decreasing the thickness the influence of the surface energy becomes dominant. The effects of the couple stress and surface parameters on the nonlinear vibration response of FG small-scale beams are slightly lower than those on the linear response.

Additionally, increasing the bulk modulus of elasticity ratio E_r increases the natural frequencies of FG micro-/nanobeams, and this effect is increased as the gradient index of SIG-FG or PL-FG is, respectively, decreases or increases. For all analyses, the frequency of SIG-FG nanobeams is higher than that of PL-FG nanobeams with $k < 1$, while the opposite is noticed with $k > 1$. Finally, neglecting any of the geometric nonlinearity, local microstructure, surface residual stress, surface elastic modulus, surface mass density, or nonclassical boundary conditions may result in an inaccurate analysis of FG micro-/nanobeams. Also, the vibration response of FG nanobeams can be controlled and optimized by the appropriate selection of the material distribution, i.e., SIG-FG or PL-FG functions, as well as the gradient index.

Appendix A: Coefficients of Eq. (41.1)

The coefficients $\mathbb{K}_1 : \mathbb{K}_5$, $\mathbb{P}_1 : \mathbb{P}_5$, and $\mathbb{M}_1 : \mathbb{M}_8$ that appear in Eq. (41.1) are defined as follows:

$$\begin{Bmatrix} \mathbb{K}_1 \\ \mathbb{K}_2 \\ \mathbb{K}_3 \\ \mathbb{K}_4 \\ \mathbb{K}_5 \end{Bmatrix} = \int_0^1 \begin{Bmatrix} \mathbb{k}_1 \phi_u \\ \mathbb{k}_2 \phi_u'' \\ \mathbb{k}_4 \left(w_s' \phi_w'' + w_s'' \phi_w' \right) + \mathbb{k}_5 \phi_w' + \mathbb{k}_6 \phi_w''' \\ \mathbb{k}_3 \phi_\psi'' + \mathbb{k}_7 \phi_\psi \\ \mathbb{k}_4 \phi_w' \phi_w'' \end{Bmatrix} \phi_u \mathrm{d}x, \tag{A.1}$$

$$\begin{Bmatrix} \mathbb{P}_1 \\ \mathbb{P}_2 \\ \mathbb{P}_3 \\ \mathbb{P}_4 \\ \mathbb{P}_5 \end{Bmatrix} = \int_0^1 \begin{Bmatrix} \mathbb{P}_1 \phi_\psi \\ \mathbb{P}_2 \phi_\psi'' + \mathbb{P}_7 \phi_\psi \\ \mathbb{P}_3 \phi_u'' \\ \mathbb{P}_4 \left(w_s' \phi_w'' + w_s'' \phi_w' \right) + \mathbb{P}_5 \phi_w' + \mathbb{P}_6 \phi_w''' \\ \mathbb{P}_4 \phi_w' \phi_w'' \end{Bmatrix} \phi_\psi \mathrm{d}x, \tag{A.2}$$

$$\begin{Bmatrix} \mathbb{M}_1 \\ \mathbb{M}_2 \\ \mathbb{M}_3 \\ \mathbb{M}_4 \end{Bmatrix} = \int_0^1 \begin{Bmatrix} \mathbb{I}_w \phi_{\mathrm{w}} \\ \mathbb{c}_0 \phi_w'' + \mathbb{c}_1 \phi_w''' + \mathbb{c}_4 \left(u_s'' \phi_w' + u_s' \phi_w'' \right) + \mathbb{c}_5 \left(\psi_s'' \phi_w' + \psi_s' \phi_w'' \right) + \mathbb{c}_6 \left(w_s'^2 \phi_w'' + 2 w_s' w_s'' \phi_w' \right) \\ \mathbb{c}_2 \phi_\psi''' + \mathbb{c}_3 \phi_\psi' + \mathbb{c}_5 \left(w_s'' \phi_\psi' + w_s' \phi_\psi'' \right) \\ \mathbb{c}_4 \left(w_s'' \phi_u' + w_s' \phi_u'' \right) \end{Bmatrix} \phi_w \mathrm{d}x, \tag{A.3}$$

$$\begin{Bmatrix} \mathbb{M}_5 \\ \mathbb{M}_6 \\ \mathbb{M}_7 \\ \mathbb{M}_8 \end{Bmatrix} = \int_0^1 \begin{Bmatrix} \mathbb{c}_4 \left(\phi_u'' \phi_w' + \phi_u' \phi_w'' \right) \\ \mathbb{c}_5 \left(\phi_\psi'' \phi_w' + \phi_\psi' \phi_w'' \right) \\ \mathbb{c}_6 \left(2 w_s' \phi_w' \phi_w'' + w_s'' \phi_w'^2 \right) \\ \mathbb{c}_6 \phi_w'^2 \phi_w'' \end{Bmatrix} \phi_w \mathrm{d}x. \tag{A.4}$$

Appendix B: Pseudo-arclength continuation

The pseudo-arclength continuation is used to find the steady-state periodic response of a Timoshenko nanobeam, Eq. (41), in a time period $T = 2\pi/\Omega_{\mathrm{NL}}$. In order to obtain this response, we define $\bar{\tau} = t/T$; afterward using a spectral collocation method, the system is discretized over the time domain $\bar{\tau}$ into an even number of periodic grid points (N_t) given by Eq. (B.1),

$$\bar{\tau} = \frac{i}{N_{\mathrm{t}}}, 0 < i < 1, \quad i = 1, 2, \ldots, N_{\mathrm{t}}. \tag{B.1}$$

Then, the discretized system will be

$$\left(\frac{\Omega_{\mathrm{NL}}}{2\pi}\right)^2 \mathbb{K}_1 D_{\mathrm{t}}^{(2)} Q_u + \mathbb{K}_2 Q_u + \mathbb{K}_3 Q_w + \mathbb{K}_4 Q_\psi + \mathbb{K}_5 (Q_w)^{\circ 2} = 0, \tag{B.2}$$

$$\left(\frac{\Omega_{\mathrm{NL}}}{2\pi}\right)^2 \mathbb{M}_1 D_{\mathrm{t}}^{(2)} Q_w + \mathbb{M}_2 Q_w + \mathbb{M}_3 Q_\psi + \mathbb{M}_4 Q_u + \mathbb{M}_5 (Q_u \circ Q_w)$$
$$+\mathbb{M}_6 \left(Q_\psi \circ Q_w\right) + \mathbb{M}_7 (Q_w)^{\circ 2} + \mathbb{M}_8 (Q_w)^{\circ 3} = 0, \tag{B.3}$$

$$\left(\frac{\Omega_{\mathrm{NL}}}{2\pi}\right)^2 \mathbb{P}_1 D_{\mathrm{t}}^{(2)} Q_\psi + \mathbb{P}_2 Q_\psi + \mathbb{P}_3 Q_u + \mathbb{P}_4 Q_w + \mathbb{P}_5 (Q_w)^{\circ 2} = 0 \tag{B.4}$$

where $(\circ)$ is the Hadamard product operator, Ω_{NL} is the nonlinear frequency to be calculated, the column vectors $\{Q_w, Q_u, Q_\psi\}$ are defined as:

$$Q_u = \left[q_{u_1}, q_{u_2}, \ldots q_{u_{N_t}}\right]^{\mathrm{T}}, \; Q_w = \left[q_{w_1}, q_{w_2}, \ldots q_{w_{N_t}}\right]^{\mathrm{T}}, \; Q_\psi = \left[q_{\psi_1}, q_{\psi_2}, \ldots q_{\psi_{N_t}}\right]^{\mathrm{T}}, \tag{B.5}$$

and $D_{\mathrm{t}}^{(2)}$ is spectral differentiation matrix operator [65].

Equations (B.2–B.4) can be rewritten in the form

$$\mathcal{F}(\boldsymbol{Q}, \Omega_{\mathrm{NL}}) = 0 \tag{B.6}$$

where $\boldsymbol{Q} = [Q_u, Q_w, Q_\psi]_{3N_t \times 1}$. In order to employ the pseudo-arclength continuation method, Eq. (B.6) is parameterized by the arclength s, such that

$$\mathcal{F}(\boldsymbol{Q}(s), \Omega_{\mathrm{NL}}(s)) = 0. \tag{B.7}$$

To obtain a new, fully determined system for the two-vector $(\boldsymbol{Q}, \Omega_{\mathrm{NL}})$, a restriction is added such that

$$\|\dot{\boldsymbol{Q}}\|^2 + \|\dot{\Omega}_{\mathrm{NL}}^2\|^2 = 1 \tag{B.8}$$

where $\dot{\boldsymbol{Q}} = \frac{\mathrm{d}Q}{\mathrm{d}s}$ and $\dot{\Omega}_{\mathrm{NL}} = \frac{\mathrm{d}\Omega}{\mathrm{d}s}$. With this restriction, we obtain a new, fully determined system for the two-vector $(\boldsymbol{Q}, \Omega_{\mathrm{NL}})$, as a function of s,

$$\begin{cases} \mathcal{F}_Q \dot{\boldsymbol{Q}} + \mathcal{F}_{\Omega_{\mathrm{NL}}} \dot{\Omega}_{\mathrm{NL}} = 0, \\ \|\dot{Q}\|^2 + \|\dot{\Omega}_{\mathrm{NL}}^2\|^2 = 1. \end{cases} \tag{B.9}$$

Then, Eq. (B.9) can be solved by a predictor–corrector method, where the Newton-type iterations in the corrector are typically restricted to be perpendicular to the solution curve being continued. Afterward, the frequency response curves, i.e., nonlinear frequency Ω_{NL} versus nonlinear amplitude Q_w, are obtained.

References

1. Udupa, G., Rao, S.S., Gangadharan, K.: Functionally graded composite materials: an overview. Procedia Mater. Sci. **5**, 1291–1299 (2014)
2. Kanani, A., Niknam, H., Ohadi, A., Aghdam, M.: Effect of nonlinear elastic foundation on large amplitude free and forced vibration of functionally graded beam. Compos. Struct. **115**, 60–68 (2014)
3. Lee, Z., Ophus, C., Fischer, L., Nelson-Fitzpatrick, N., Westra, K., Evoy, S., Radmilovic, V., Dahmen, U., Mitlin, D.: Metallic NEMS components fabricated from nanocomposite Al–Mo films. Nanotechnology **17**(12), 3063 (2006)
4. Witvrouw A., Mehta, A.: The use of functionally graded poly-SiGe layers for MEMS applications. In: Materials Science Forum. Trans Tech Publications (2005)
5. Al-Basyouni, K., Tounsi, A., Mahmoud, S.: Size dependent bending and vibration analysis of functionally graded micro beams based on modified couple stress theory and neutral surface position. Compos. Struct. **125**, 621–630 (2015)
6. Arbind, A., Reddy, J., Srinivasa, A.: Modified couple stress-based third-order theory for nonlinear analysis of functionally graded beams. Latin Am. J. Solids Struct. **11**(3), 459–487 (2014)
7. Khorshidi, M.A., Shariati, M., Emam, S.A.: Postbuckling of functionally graded nanobeams based on modified couple stress theory under general beam theory. Int. J. Mech. Sci. **110**, 160–169 (2016)
8. Shanab, R.A., Attia, M.A., Mohamed, S.A.: Nonlinear analysis of functionally graded nanoscale beams incorporating the surface energy and microstructure effects. Int. J. Mech. Sci. **131**, 908–923 (2017)
9. Thai, H.-T., Vo, T.P., Nguyen, T.-K., Lee, J.: Size-dependent behavior of functionally graded sandwich microbeams based on the modified couple stress theory. Compos. Struct. **123**, 337–349 (2015)

10. Trinh, L.C., Nguyen, H.X., Vo, T.P., Nguyen, T.-K.: Size-dependent behaviour of functionally graded microbeams using various shear deformation theories based on the modified couple stress theory. Compos. Struct. **154**, 556–572 (2016)
11. Attia, M.A., Emam, S.A.: Electrostatic nonlinear bending, buckling and free vibrations of viscoelastic microbeams based on the modified couple stress theory. Acta Mech. **229**(8), 3235–3255 (2018)
12. Ghayesh, M.H.: Functionally graded microbeams: simultaneous presence of imperfection and viscoelasticity. Int. J. Mech. Sci. **140**, 339–350 (2018)
13. Shafiei, N., Mousavi, A., Ghadiri, M.: Vibration behavior of a rotating non-uniform FG microbeam based on the modified couple stress theory and GDQEM. Compos. Struct. **149**, 157–169 (2016)
14. Şimşek, M., Reddy, J.: Bending and vibration of functionally graded microbeams using a new higher order beam theory and the modified couple stress theory. Int. J. Eng. Sci. **64**, 37–53 (2013)
15. Gurtin, M.E., Murdoch, A.I.: A continuum theory of elastic material surfaces. Arch. Ration. Mech. Anal. **57**(4), 291–323 (1975)
16. Gurtin, M.E., Murdoch, A.I.: Surface stress in solids. Int. J. Solids Struct. **14**(6), 431–440 (1978)
17. Amirian, B., Hosseini-Ara, R., Moosavi, H.: Surface and thermal effects on vibration of embedded alumina nanobeams based on novel Timoshenko beam model. Appl. Math. Mech. **35**(7), 875–886 (2014)
18. Ansari, R., Mohammadi, V., Shojaei, M.F., Gholami, R., Rouhi, H.: Nonlinear vibration analysis of Timoshenko nanobeams based on surface stress elasticity theory. Eur. J. Mech. A/Solids **45**, 143–152 (2014)
19. Ansari, R., Mohammadi, V., Shojaei, M.F., Gholami, R., Sahmani, S.: On the forced vibration analysis of Timoshenko nanobeams based on the surface stress elasticity theory. Compos. B Eng. **60**, 158–166 (2014)
20. Attia, M.A.: On the mechanics of functionally graded nanobeams with the account of surface elasticity. Int. J. Eng. Sci. **115**, 73–101 (2017)
21. Dai, H., Zhao, D., Zou, J., Wang, L.: Surface effect on the nonlinear forced vibration of cantilevered nanobeams. Physica E **80**, 25–30 (2016)
22. Gao, X.L.: A new Timoshenko beam model incorporating microstructure and surface energy effects. Acta Mech. **226**(2), 457–474 (2015)
23. Gao, X.L., Mahmoud, F.: A new Bernoulli-Euler beam model incorporating microstructure and surface energy effects. Zeitschrift für angewandte Mathematik und Physik ZAMP **65**(2), 393–404 (2014)
24. Gheshlaghi, B., Hasheminejad, S.M.: Surface effects on nonlinear free vibration of nanobeams. Compos. B Eng. **42**(4), 934–937 (2011)
25. Hosseini-Hashemi, S., Nazemnezhad, R.: An analytical study on the nonlinear free vibration of functionally graded nanobeams incorporating surface effects. Compos. B Eng. **52**, 199–206 (2013)
26. Hosseini-Hashemi, S., Nazemnezhad, R., Bedroud, M.: Surface effects on nonlinear free vibration of functionally graded nanobeams using nonlocal elasticity. Appl. Math. Model. **38**(14), 3538–3553 (2014)
27. Hosseini-Hashemi, S., Nazemnezhad, R., Rokni, H.: Nonlocal nonlinear free vibration of nanobeams with surface effects. Eur. J. Mech. A/Solids **52**, 44–53 (2015)
28. Kasirajan, P., Amirtham, R., Reddy, J.N.: Surface and non-local effects for non-linear analysis of Timoshenko beams. Int. J. Non-Linear Mech. **76**, 100–111 (2015)
29. Nazemnezhad, R., Hosseini-Hashemi, S.: Nonlinear free vibration analysis of Timoshenko nanobeams with surface energy. Meccanica **50**(4), 1027–1044 (2015)
30. Ansari, R., Pourashraf, T., Gholami, R.: An exact solution for the nonlinear forced vibration of functionally graded nanobeams in thermal environment based on surface elasticity theory. Thin-Walled Struct. **93**, 169–176 (2015)
31. Hosseini-Hashemi, S., Nahas, I., Fakher, M., Nazemnezhad, R.: Surface effects on free vibration of piezoelectric functionally graded nanobeams using nonlocal elasticity. Acta Mech. **225**(6), 1555–1564 (2014)
32. Wang, G.-F., Feng, X.-Q.: Timoshenko beam model for buckling and vibration of nanowires with surface effects. J. Phys. D Appl. Phys. **42**(15), 155411 (2009)
33. Eltaher, M., Mahmoud, F., Assie, A., Meletis, E.: Coupling effects of nonlocal and surface energy on vibration analysis of nanobeams. Appl. Math. Comput. **224**, 760–774 (2013)
34. Sahmani, S., Bahrami, M., Ansari, R.: Surface energy effects on the free vibration characteristics of postbuckled third-order shear deformable nanobeams. Compos. Struct. **116**, 552–561 (2014)
35. Wang, K., Zeng, S., Wang, B.: Large amplitude free vibration of electrically actuated nanobeams with surface energy and thermal effects. Int. J. Mech. Sci. **131**, 227–233 (2017)
36. Ghadiri, M., Shafiei, N., Akbarshahi, A.: Influence of thermal and surface effects on vibration behavior of nonlocal rotating Timoshenko nanobeam. Appl. Phys. A **122**(7), 673 (2016)
37. Attia, M.A., Rahman, A.A.A.: On vibrations of functionally graded viscoelastic nanobeams with surface effects. Int. J. Eng. Sci. **127**, 1–32 (2018)
38. Oskouie, M.F., Ansari, R.: Linear and nonlinear vibrations of fractional viscoelastic Timoshenko nanobeams considering surface energy effects. Appl. Math. Model. **43**, 337–350 (2017)
39. Fang, X.-Q., Zhu, C.-S., Liu, J.-X., Liu, X.-L.: Surface energy effect on free vibration of nano-sized piezoelectric double-shell structures. Physica B **529**, 41–56 (2018)
40. Zhu, C.-S., Fang, X.-Q., Liu, J.-X., Li, H.-Y.: Surface energy effect on nonlinear free vibration behavior of orthotropic piezoelectric cylindrical nano-shells. Eur. J. Mech. A/Solids **66**, 423–432 (2017)
41. Rouhi, H., Ansari, R., Darvizeh, M.: Exact solution for the vibrations of cylindrical nanoshells considering surface energy effect. J. Ultrafine Grained Nanostruct. Mater. **48**(2), 113–124 (2015)
42. Gao, X.L., Zhang, G.: A microstructure- and surface energy-dependent third-order shear deformation beam model. Zeitschrift für angewandte Mathematik und Physik ZAMP **66**(4), 1871–1894 (2015)
43. Zhang, L., Wang, B., Zhou, S., Xue, Y.: Modeling the size-dependent nanostructures: incorporating the bulk and surface effects. J. Nanomech. Micromech. **7**(2), 04016012 (2016)
44. Shaat, M., Mohamed, S.A.: Nonlinear-electrostatic analysis of micro-actuated beams based on couple stress and surface elasticity theories. Int. J. Mech. Sci. **84**, 208–217 (2014)

45. Attia, M.A., Mahmoud, F.F.: Modeling and analysis of nanobeams based on nonlocal-couple stress elasticity and surface energy theories. Int. J. Mech. Sci. **105**, 126–134 (2016)
46. Shaat, M., Mahmoud, F.F., Gao, X.L., Faheem, A.F.: Size-dependent bending analysis of Kirchhoff nano-plates based on a modified couple-stress theory including surface effects. Int. J. Mech. Sci. **79**, 31–37 (2014)
47. Wang, K., Kitamura, T., Wang, B.: Nonlinear pull-in instability and free vibration of micro/nanoscale plates with surface energy—a modified couple stress theory model. Int. J. Mech. Sci. **99**, 288–296 (2015)
48. Wang, K., Wang, B., Zhang, C.: Surface energy and thermal stress effect on nonlinear vibration of electrostatically actuated circular micro-/nanoplates based on modified couple stress theory. Acta Mech. **228**(1), 129–140 (2017)
49. Zhang, G., Gao, X.-L., Wang, J.: A non-classical model for circular Kirchhoff plates incorporating microstructure and surface energy effects. Acta Mech. **226**(12), 4073–4085 (2015)
50. Gao, X.L., Zhang, G.: A non-classical Kirchhoff plate model incorporating microstructure, surface energy and foundation effects. Continuum Mech. Thermodyn. **28**(1–2), 195–213 (2016)
51. Attia, M.A., Mahmoud, F.F.: Size-dependent behavior of viscoelastic nanoplates incorporating surface energy and microstructure effects. Int. J. Mech. Sci. **123**, 117–132 (2017)
52. Nazemnezhad, R., Hosseini-Hashemi, S.: Nonlocal nonlinear free vibration of functionally graded nanobeams. Compos. Struct. **110**, 192–199 (2014)
53. Tang, Y.-G., Liu, Y., Zhao, D.: Effects of neutral surface deviation on nonlinear resonance of embedded temperature-dependent functionally graded nanobeams. Compos. Struct. **184**, 969–979 (2018)
54. Şimşek, M.: Nonlinear free vibration of a functionally graded nanobeam using nonlocal strain gradient theory and a novel Hamiltonian approach. Int. J. Eng. Sci. **105**, 12–27 (2016)
55. Chi, S.-H., Chung, Y.-L.: Mechanical behavior of functionally graded material plates under transverse load—part I: analysis. Int. J. Solids Struct. **43**(13), 3657–3674 (2006)
56. Reddy, J.N.: Mechanics of Laminated Composite Plates and Shells: Theory and Analysis. CRC Press, Boca Raton (2003)
57. Attia, M.A., Mahmoud, F.F.: Analysis of viscoelastic Bernoulli–Euler nanobeams incorporating nonlocal and microstructure effects. Int. J. Mech. Mater. Des. **13**(3), 385–406 (2017)
58. Attia, M.A.: Investigation of size-dependent quasistatic response of electrically actuated nonlinear viscoelastic microcantilevers and microbridges. Meccanica **52**(10), 2391–2420 (2017)
59. Attia, M.A., Mohamed, S.A.: Nonlinear modeling and analysis of electrically actuated viscoelastic microbeams based on the modified couple stress theory. Appl. Math. Model. **41**, 195–222 (2017)
60. Hutchinson, J.: Shear coefficients for Timoshenko beam theory. J. Appl. Mech. **68**(1), 87–92 (2001)
61. Yang, F., Chong, A., Lam, D.C.C., Tong, P.: Couple stress based strain gradient theory for elasticity. Int. J. Solids Struct. **39**(10), 2731–2743 (2002)
62. Sahmani, S., Aghdam, M., Bahrami, M.: On the free vibration characteristics of postbuckled third-order shear deformable FGM nanobeams including surface effects. Compos. Struct. **121**, 377–385 (2015)
63. Quan, J., Chang, C.: New insights in solving distributed system equations by the quadrature method—I. Analysis. Comput. Chem. Eng. **13**(7), 779–788 (1989)
64. Ke, L.-L., Yang, J., Kitipornchai, S.: An analytical study on the nonlinear vibration of functionally graded beams. Meccanica **45**(6), 743–752 (2010)
65. Trefethen, L.N.: Spectral methods in MATLAB, vol. 10. SIAM, New Delhi (2000)
66. Mittelmann, H.D.: A pseudo-arclength continuation method for nonlinear eigenvalue problems. SIAM J. Numer. Anal. **23**(5), 1007–1016 (1986)
67. Mohamed, S.A., Shanab, R.A., Seddek, L.: Vibration analysis of Euler–Bernoulli nanobeams embedded in an elastic medium by a sixth-order compact finite difference method. Appl. Math. Model. **40**(3), 2396–2406 (2016)
68. Reddy, J.: Microstructure-dependent couple stress theories of functionally graded beams. J. Mech. Phys. Solids **59**(11), 2382–2399 (2011)
69. Ebrahimi, F., Salari, E.: Size-dependent free flexural vibrational behavior of functionally graded nanobeams using semi-analytical differential transform method. Compos. B Eng. **79**, 156–169 (2015)
70. Eltaher, M., Emam, S.A., Mahmoud, F.: Free vibration analysis of functionally graded size-dependent nanobeams. Appl. Math. Comput. **218**(14), 7406–7420 (2012)
71. Hamed, M., Eltaher, M., Sadoun, A., Almitani, K.: Free vibration of symmetric and sigmoid functionally graded nanobeams. Appl. Phys. A **122**(9), 829 (2016)
72. Liu, C., Rajapakse, R.: Continuum models incorporating surface energy for static and dynamic response of nanoscale beams. IEEE Trans. Nanotechnol. **9**(4), 422–431 (2009)
73. Zhang, G., Gao, X.-L., Bishop, J., Fang, H.: Band gaps for elastic wave propagation in a periodic composite beam structure incorporating microstructure and surface energy effects. Compos. Struct. **189**, 263–272 (2018)
74. Ma, H., Gao, X.L., Reddy, J.: A microstructure-dependent Timoshenko beam model based on a modified couple stress theory. J. Mech. Phys. Solids **56**(12), 3379–3391 (2008)
75. Ansari, R., Gholami, R., Sahmani, S.: Free vibration analysis of size-dependent functionally graded microbeams based on the strain gradient Timoshenko beam theory. Compos. Struct. **94**(1), 221–228 (2011)
76. Aghazadeh, R., Cigeroglu, E., Dag, S.: Static and free vibration analyses of small-scale functionally graded beams possessing a variable length scale parameter using different beam theories. Eur. J. Mech. A/Solids **46**, 1–11 (2014)
77. Chen, X., Zhang, X., Lu, Y., Li, Y.: Static and dynamic analysis of the postbuckling of bi-directional functionally graded material microbeams. Int. J. Mech. Sci. **151**, 424–443 (2019)
78. Chen, X., Lu, Y., Li, Y.: Free vibration, buckling and dynamic stability of bi-directional FG microbeam with a variable length scale parameter embedded in elastic medium. Appl. Math. Model. **67**, 430–448 (2019)
79. Lam, D.C., Yang, F., Chong, A., Wang, J., Tong, P.: Experiments and theory in strain gradient elasticity. J. Mech. Phys. Solids **51**(8), 1477–1508 (2003)
80. Nix, W.D., Gao, H.: Indentation size effects in crystalline materials: a law for strain gradient plasticity. J. Mech. Phys. Solids **46**(3), 411–425 (1998)

81. Maranganti, R., Sharma, P.: A novel atomistic approach to determine strain-gradient elasticity constants: Tabulation and comparison for various metals, semiconductors, silica, polymers and the (ir) relevance for nanotechnologies. J. Mech. Phys. Solids **55**(9), 1823–1852 (2007)